공학석사 학위논문

Self-Learning Data-Driven Yield Criteria for Anisotropic Materials

비등방성 재료에 대한 자가 학습 데이터 기반의 항복 조건

2019 년 8 월

서울대학교 대학원

기계항공공학부

장 경 석

Self-Learning Data-Driven Yield Criteria for anisotropic Materials

비등방성 재료에 대한 자가 학습 데이터 기반의 항복 조건

지도 교수 윤 군 진

이 논문을 공학석사 학위논문으로 제출함
2019 년 8 월

서울대학교 대학원
기계항공공학부
장 경 석

장경석의 공학석사 학위논문을 인준함
2019 년 8 월

위 원 장 신 상 준 (인)

부위원장 윤 군 진 (인)

위 원 김 용 협 (인)

Abstract

Self-Learning Data-Driven Yield Criteria for Anisotropic Materials

Kyungsuk Jang
Department of Mechanical and Aerospace Engineering
The Graduate School
Seoul National University

Yield criteria have been one of the essential theories for structural analysis to prevent undesirable material behaviors. Although the theories have been developed with high accuracy, many anisotropic parameters are necessary to complete anisotropic yield equations. Many experimental tests are required to obtain them due to uncertainty of anisotropic materials. The major purpose of this thesis is to propose a new methodology that can identify anisotropic yield criterion of uncharacterized new materials. The new methodology creates new yield criteria by means of two subsequent steps: 1) self-learning inverse finite element (SELIFE) simulations with minimal experimental measurements and 2) data-driven mechanics approach. SELIFE can self-learn stress-strain time

histories of any material behavior based on boundary reaction forces, displacements and/or internal displacements from experiments. Self-learning capability of material behavior in the SELIFE analysis is enabled through adaptive progressive training of artificial neural network (ANN)-based material constitutive models. From the self-learned stress-strain data, sufficient initial yield stresses were extracted in comprehensive stress increment directions. This is called data-processing step. Following the data-processing, symbolic regression via genetic programming is performed to derive a new data-driven anisotropic yield criterion. For an example, Hill's anisotropic yield criterion is used, which is assumed as unknown. A biaxial specimen was modeled subjected to four displacement boundary conditions to get sufficient initial yield stress data. Finally, the biaxial simulation was conducted with the data-driven yield criterion in ABAQUS for verification. Through SELIFE simulation and data-driven mechanics approach, a new anisotropic yield criterion was obtained and compared with reference yield criteria.

Keywords : Data-driven Mechanics, artificial neural networks, genetic program, anisotropic yield criterion, initial yield stress, biaxial specimen

Student Number : 2017-27307

Table of contents

List of figures

List of tables

1. Introduction

1.1. Background and Motivation

Yield criteria have been developed to define the initiation of plastic deformation with complex loading conditions and used in a variety of structural engineering applications. Several representations for the isotropic yield surface have been proposed by Tresca, Von Mises [1], and Hosford [2]. Anisotropic yield surfaces in stress space have also been studied by many researchers such as Hill [3-5], Bassani [6], and Budiansky [7]. The theories to describe an anisotropic initial yielding behavior are required to predict failure prevention of structures and provide engineers with information about the limit of elastic deformation. However, there are still challenges associated with developing comprehensive yield criteria for anisotropic material. Many efforts and costs are needed to fit anisotropic parameters because of uncertainties from material properties in any structures. In this paper, we propose a new methodology for developing new yield criteria by using data-driven mechanics and genetic programming.

The self-learning data-driven mechanics should be emphasized that it is able to train data itself by generating ample stress-strain data from minimal experimental data and physics-based laws. This capability of self-learning data-driven mechanics is unprecedented. To demonstrate the ability of the proposed self-learning data-driven mechanics, biaxial specimens made of anisotropic metal were accepted with four boundary conditions. The proposed methodology can self-learn any material behavior regardless of both elastic and plastic characteristics.

1.2. Objectives and Thesis Overview

In this study, we aim to open a new research philosophy and radical direction to discover new yield criteria for an anisotropic metal under complex stress states. The proposed methodology is based on finite element model with artificial neural network based material constitutive model, self-learning yield stress data of anisotropic metal and mathematical formulation by evolutionary genetic programming. The method consists of three major sequential steps: Step 1) inverse identification of stress-strain data from self-learning data-driven mechanics, Step 2) data analysis called the

Data-processing to obtain yield stresses from the stress-strain curves without any conventional yield criteria and Step 3) derivation and formulation of physics-based law from mathematical symbolic regression based on genetic programming. The driven equation is in terms of the initial yield stress and the yield stress components which is discovered from the Step 2). Finally, data-driven criteria is able to obtain from the Step 3). Finally, in Step 4), data-driven criteria can be obtained. Overview of the thesis is shown in Figure 1.1.

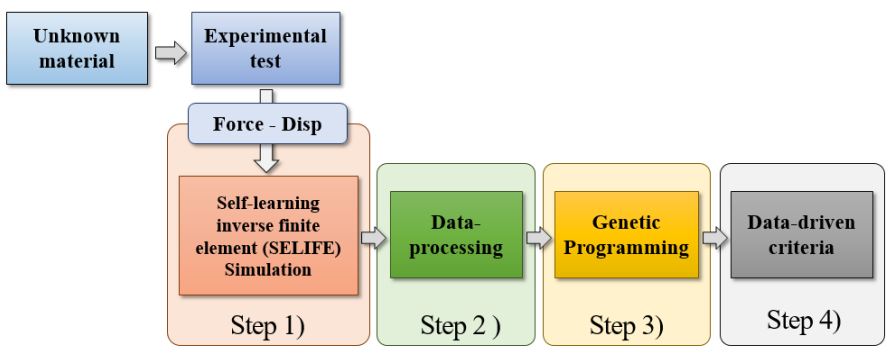

Figure 1.1 Overview

The proposed methodology has significant meaning. The methodology can establish any criteria based on experimental test data i.e. force and displacement measurements from unknown material. In this thesis, a biaxial model is especially assumed that its material property can be following Hill's 48 anisotropic yield criterion.

2. Data-Driven Mechanics and Artificial Neural Network Material Models

2.1. Data-Driven Mechanics

Data-driven mechanics is one of the branch where the underlying laws such as constraints, material constitutive law or conservation law are replaced or collaborated with the experimental data in non-conventional schemes. Material constitutive law is relatively more subjected to errors or uncertainties than other entailed physics-based law associated with boundary value problems. Therefore, data-driven approach to the material constitutive modeling is considered as an unprecedented idea and relatively new promising direction. For example, Kirchdoerfer et al. proposed computational algorithmic approach that can realize data-driven modeling of material constitutive laws within the finite element analysis framework [8]. Data from experiment tests have been mainly used for parameter identification [9] or model updating within the empiricism regime rather than replacing those laws or constraints in the boundary value problems. In regards to material experimental data, material informatics [10] entails applications of various

statistical techniques such as principal component analysis, and artificial intelligence such as neural network [11]; deep learning [12], support vector machine [13], etc. Many researchers have used statistical methods to apply to various research fields such as multiscale material modeling [14-16], cyclic plasticity [17], nonlinear multi-axial stress-strain behaviors of fiber-reinforced plastic composites [18], rubber materials [19], and rate-dependent materials [20]. Artificial intelligence in surrogate-type model has shown superior predictability of materials' physical properties based on experimental data.

2.2. Artificial Neural Network Materials Models

On the other hand, artificial neural network (ANN) has also been applied for substituting the empirical material constitutive models as knowledge-based material constitutive model [21-25]. ANN material models are able to predict the nonlinear multi-axial stress-strain relationships both under monotonic and cyclic loading [26]. Intrusive implementation technique of ANN material constitutive model within finite element analysis codes is available [26, 27].The ANN for knowledge based constitutive model has current strain, one

or a few prehistoric strains, and other internal variables as inputs and current stresses as output values so that they can be implemented in conventional nonlinear finite element tests. However, difficulty about ANN material model is preparations for comprehensive training data from experiments, which is formidable in usual material tests. For tackling such challenges of ANN models, Ghaboussi, et al. proposed an online training methodology called an autoprogressive training whereby ANN material constitutive models are automatically trained during nonlinear finite element analyses subjected to experimental boundary reaction forces and displacements [28]. This innovative idea has an advantage of generating sufficient stress–strain training data from minimal experimental measurements. Following work, Yun et al. proposed a strategic methodology for developing nonlinear material constitutive models by combining the online autoprogressive training of ANN material constitutive models with a symbolic regression, i.e., genetic programming technique [29]. Symbolic regression technique such as genetic programming is a useful approach for generating mathematical equations from experimental data [29]. Most of ANN material models are surrogate–type

predictive black box models for specific physical properties or material constitutive models that can predict nonlinear stress–strain relationships. The capability of ANN material models with the online autoprogressive training is far beyond inversely finding nonlinear stress–strain relationship. However, very few researches on its application to ANN based data–driven mechanics. As aforementioned, our focus is the application of ANN to development of new anisotropic initial yield criterion.

3. Self-Learning Inverse Finite Element (SELIFE) Simulation

3.1. ANN-Based Material Constitutive Model for Anisotropic Materials

In order to achieve the single−valuedness between inputs and outputs of the hysteretic ANN−based constitutive model, one internal variable is included [30]. The internal variable has the physical meaning of strain energy density. The ANN−based material model is defined as following :

$$\boldsymbol{\sigma}_{\mathrm{n}} = \boldsymbol{\sigma}_{\mathrm{NN}}([\boldsymbol{\varepsilon}_n, \boldsymbol{\varepsilon}_{n-1}, \boldsymbol{\sigma}_{n-1}, \varsigma_n]; [NN\ Architecture]) \qquad (1)$$

where $\varsigma_n = \sigma_{n-1}\varepsilon_{n-1} + \sigma_{n-1}\Delta\varepsilon_n$ is internal variable

Stress data from finite element analysis are fed into the ANN recursively to make it robust from errors [30]. Hyperbolic tangent function was implemented for an activation function in the ANN and adaptive backpropagation called resilient back−propagation (RPROP) was accepted for the error backpropagation [31]. Figure 3.1 describes the architecture of ANN; input and output node, two hidden layers, and the activation function (hyperbolic tangent function). Moreover, some ANN parameters are added as well; weight

connections between each of the layers ($w_{ik}^{\sigma C}, w_{kl}^{CB}, w_{lj}^{B\varepsilon}$, and w_{lj}^{BSV}).

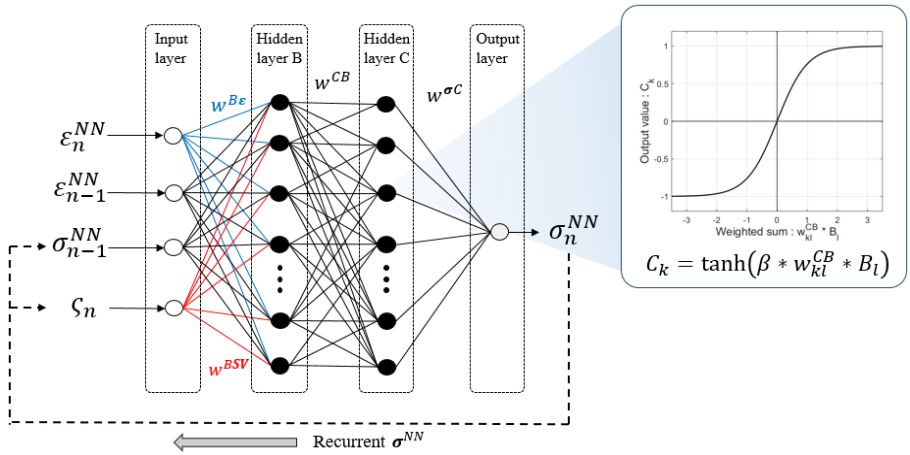

Figure 3.1 The architecture of artificial neural network

During the ANN-based FEA, ABAQUS calls the special user subroutine which the ANN is inserted in order to predict stress values and calculate material tangent stiffness matrix (Jacobian matrix). It is updated using an explicit expression which is a function of inputs and outputs as well as the ANN parameters such as weight factors ($w_{ik}^{\sigma C}, w_{kl}^{CB}, w_{lj}^{B\varepsilon}$, and w_{lj}^{BSV}), scale factors (S_i^{σ} and S_j^{ε}), the derivation form of the activation function ($(1 - f(\bullet)^2)$) and the activation function values from each of the hidden layers in the given ANN (${}^{n+1}\boldsymbol{\sigma}_i^{NN}$, ${}^{n+1}C_k$, and ${}^{n+1}B_l$). Therefore, the Jacobian matrix [32] is formulated in terms of ANN parameters as following :

$$
\begin{aligned}
D_{NN,ij}^{ep} &= \frac{\partial \Delta^{n+1}\boldsymbol{\sigma}_i}{\partial \Delta^{n+1}\boldsymbol{\varepsilon}_j} \\
&= \frac{S_i^{\boldsymbol{\sigma}}}{S_j^{\boldsymbol{\varepsilon}}}\beta^3 \sum_{k=1}^{NC}\Bigg(\left\{\left(1-\left({}^{n+1}\boldsymbol{\sigma}_i^{NN}\right)^2\right) w_{ik}^{\sigma C}\right\} \\
&\qquad \times \left[\sum_{l=1}^{NB}\left\{\left(1-\left({}^{n+1}C_k\right)^2\right) w_{kl}^{CB}\right\}\right. \\
&\qquad \left.\times\left\{\left(1-\left({}^{n+1}B_l\right)^2\right)\left(w_{lj}^{B\boldsymbol{\varepsilon}} + w_{lj}^{B\boldsymbol{SV}}\,{}^{n}\boldsymbol{\sigma}_i^{NN}\right)\right\}\right]\Bigg)
\end{aligned}
\qquad (2)
$$

3.2. Auto-Adaptive Training of ANN-Based Model

Experimental boundary measurements i.e. reaction forces and displacements from a structural or material tests are required for SELIFE simulations. Moreover, measured internal displacement field data from a digital image correlation (DIC) equipment enhance an accuracy of SELIFE. In this thesis, experimental data were substituted with displacement and force data of experimental reference simulations in order to compare the results from the reference simulations with those from SELIFE.

SELIFE requires three additional iteration loops, which are NN pass, NN step, and auto−adaptive training cycle. Sweeping all load steps is called one NN Pass. Multiple NN passes are necessary since

the ANN-based material model may not be trained with one NN pass. In each of the load incremental steps, SELIFE runs two independent finite element analysis. Force-controlled analysis (FEM-A) and displacement-controlled analysis (FEM-B) are performed individually in each of the auto-adaptive training cycles The stresses and strains are appended from FEM-A and FEM-B, respectively. Based on the SELIFE hypotheses, stress data are extracted from FEM-A while strains do from FEM-B. Multiple auto-adaptive cycles are performed until the predetermined number is reached or a convergence criterion is satisfied [33]. The displacement error, which is difference between computed displacement from FEM-A and the measured displacement, is checked as the criterion in each of the auto-adaptive cycles. In this thesis, internal displacement data are, especially, included in the displacement error calculation. A computational flow chart, which includes the three additional loops for SELIFE, is depicted in Figure 3.2.

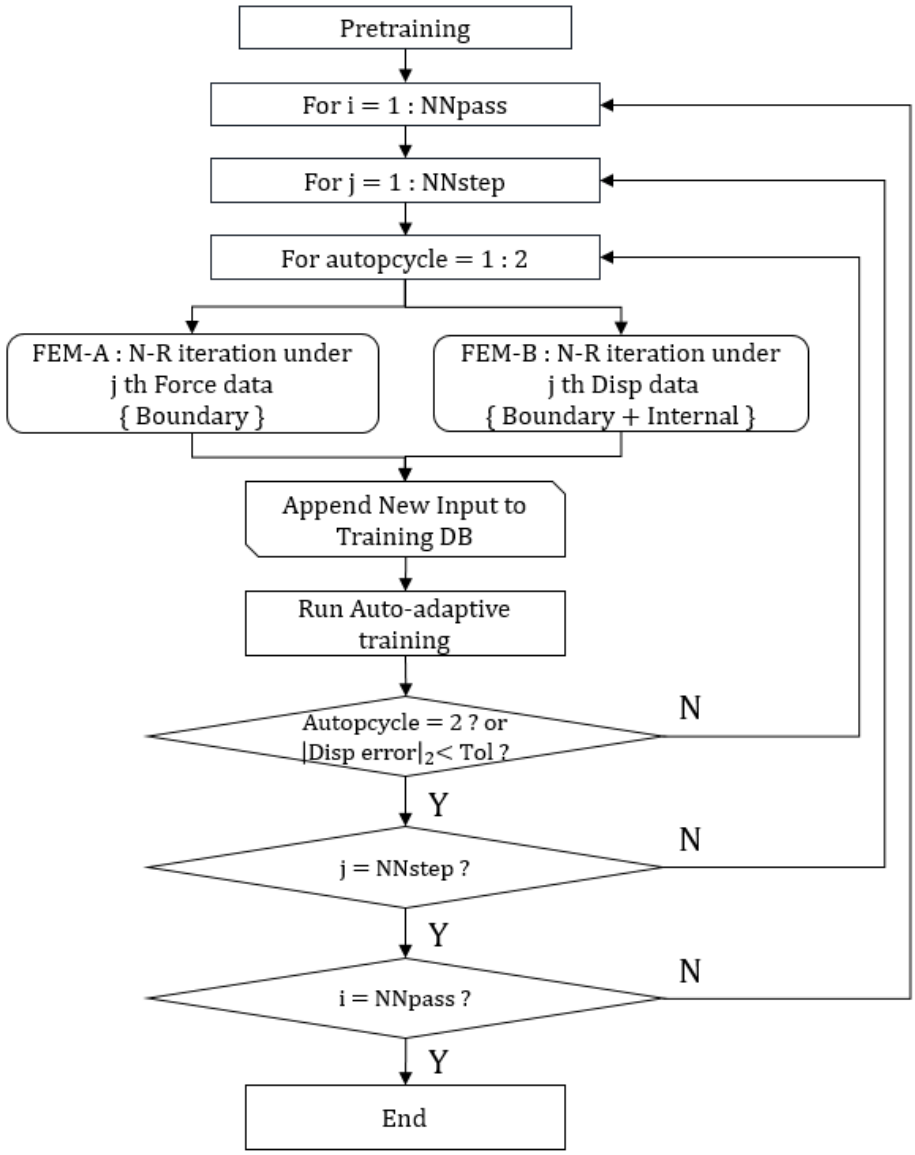

Figure 3.2 Flow chart for SELIFE simulation

Schematic algorithm is contained for detail illustration of SELIFE procedure in Figure 3.3. Rather than executing SELIFE without the pretraining process, using pretraining data is recommend for accurate results and faster convergence. The pretraining data could be generated within linear elastic strain region [32] with assumed elastic material properties or be prepared from experiment test data in Figure 3.3 (a). A user defined ANN model is updated with the pretraining data (Figure 3.3 (c)) to approximate elastic behavior (Figure 3.3 (d)). Two ANN-based finite element models are prepared in ABAQUS. One is subjected to the measured boundary reaction forces called FEM-A (Figure 3.3 (e-a)). On the other hand, the other is under the measured boundary deformations called FEM-B (Figure 3.3 (e-b)). In the first NN step of SELIFE, the updated ANN from the pretraining data can execute finite element analysis with the first load steps of experimental data (i.e. force boundary and displacement boundary) until satisfying the convergence conditions of auto-adaptive training. After ANN-based FEA, stress data from FEM-A and strain data from FEM-B are extracted, respectively (Figure 3.3 (f)). The stress-strain pairs are appended

(Figure 3.3 (g)) in the training data set (Figure 3.3 (b)). ANN model is gradually updated (Figure 3.3 (c)) by training data set with appended dataset. This procedure is repeated until the last load step.

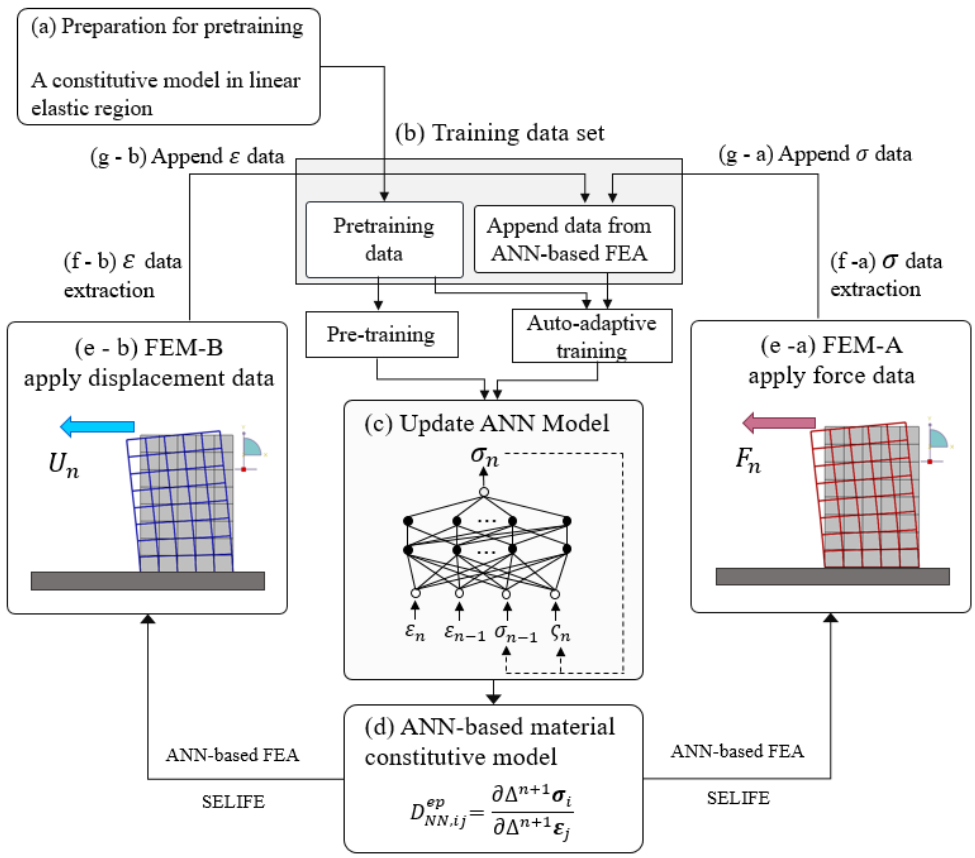

Figure 3.3 Schematic algorithm of SELIFE simulation

In Figure 3.4, the iter1 and iter2 indicate gradual training of the ANN model toward true stress−strain response through the auto adaptive training. During the SELIFE, stress−strain history data at all material points are appended into the training database. After SELIFE training, the ANN model can be used in forward nonlinear FE analysis. The concept of SELIFE generates material Big Data in terms of stress−strain history data. Since function of ANN is the primary components of the SELIFE analysis, ANN−based material model will be highlighted.

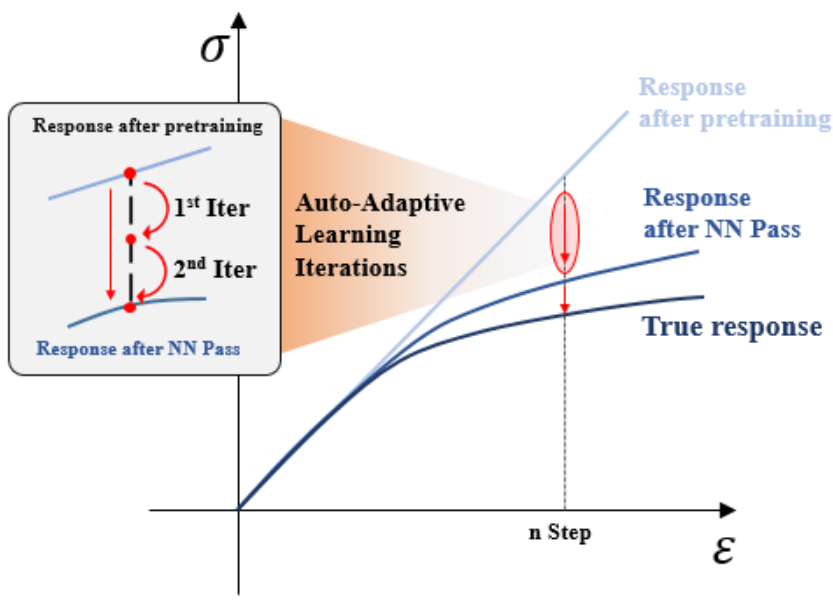

Figure 3.4 Schematic ANN model's auto-adaptive learning for true material response

4. Self-Learning Data-Driven Mechanics

4.1. Data-Processing Algorithm

To formulate appropriate data-driven yield criterion, the initial yield stress data are necessary to be collected from all cases of SELIFE. Data analysis, which we called Data-processing, discovers yield stresses from stress-strain history without any conventional yield criteria. The Data-processing is based on dealing with tangent stiffness within stress-strain curves. The Data-processing algorithm consists of two steps. The first step classifies plastic history cases and elastic history cases from whole SELIFE data. Next, the second step of the Data-processing determines which point can be the yield stress point within whole range of the stress history.

The first step of Data-processing is shown in Figure 4.1. In the beginning of the first step, stress and strain data are interpolated with specific number for proper calculation of tangent stiffness called interpolated tangent stiffness. The number of 50000 was used to interpolate stress- strain history in this study. Next, interpolated tangent stiffness is calculated with the interpolated stress- strain history by the following equation (3). Moreover, initial tangent

stiffness (4) is calculated based on the interpolated tangent stiffness of the first two percent within whole interpolation interval.

The main key point of the first step of the Data-processing is using an averaged ratio of tangent stiffness (6). It is able to classify whether stress data is plastic history or elastic history. The values of averaged ratio of tangent stiffness are one if the 1st step of the Data-processing was conducted with the elastic stress history cases because equations (3) and (4) were close to each other. However, the values of (6) are out of one if the 1st step of the Data processing was performed with the plastic stress history cases since interpolated tangent stiffness values (3) are consistently changed from the initial yield points. Therefore, the average of ratio of tangent stiffness can separate plastic stress history cases from whole stress histories. However, there is a limitation to find yield points only using this step. A determination process of yield points needs to obtain them from all plastic stress history cases.

$$\Delta^{i} = \frac{\sigma^{i+1} - \sigma^{i}}{\epsilon^{i+1} - \epsilon^{i}} \quad (i \in (1, 2, \ldots, N-1)) \tag{3}$$

$$\underline{\Delta} = \frac{\sum_{j=1}^{n} \Delta^{j}}{n} \tag{4}$$

$$\delta^i = \frac{\Delta^{\mathrm{i}}}{\underline{\Delta}} \quad (i \in (1, 2 \ldots, \mathrm{N}-1)) \tag{5}$$

$$< \delta >= \frac{\sum_{i=1}^{N-1} \delta^{\mathrm{i}}}{N} \tag{6}$$

where $\boldsymbol{n}$ describes the size of the first two percent of interpolation interval and $\mathbf{N}$ indicates the size of the interpolation number.

(a)

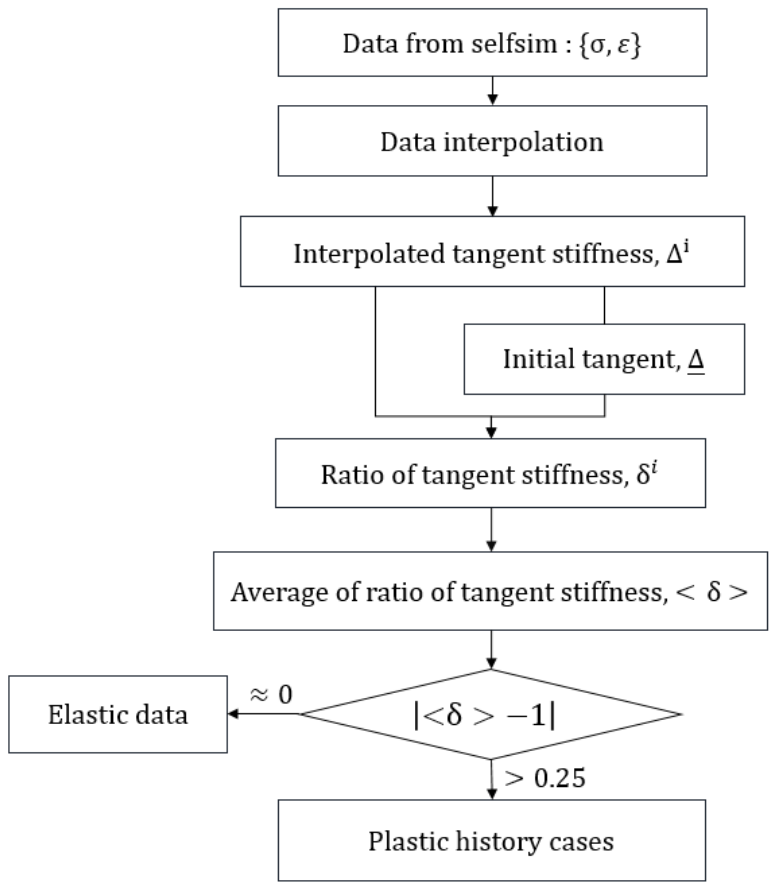

(b)

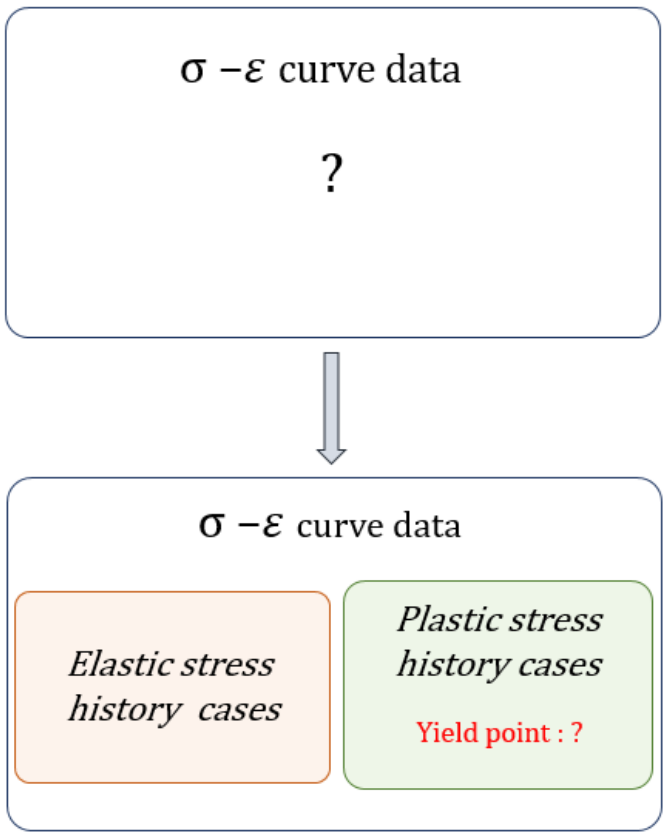

Figure 4.1 The first step of the Data-processing; (a) Flowchart for division plastic data from all SELIFE data (b) schematic diagram to obtain plastic cases

Finally, yield points from the plastic history cases can be captured by using the second step of the Data−processing. Yield points were more prominently discovered from major stress component than weak stress component. Therefore, comparison of stress components to get the major stress was necessary. Instead of using ratio of tangent stiffness (5) itself, $\left|\delta^{i}-1\right|$ was used to

capture the first deviating point from the initial tangent stiffness. Generally, the value about 0.7 for $\left|\delta^{i}-1\right|$ was appreciable to obtain the initial yield stresses from the group which characterizes plastic behaviors. More detail description about the second step of the Data-processing is shown in Figure 4.2 (a) and (b).

(a)

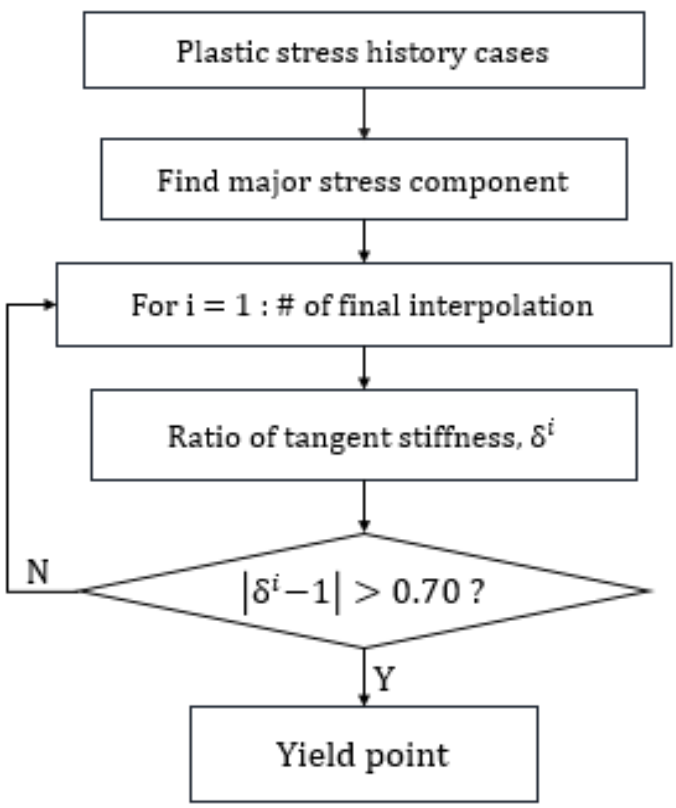

(b)

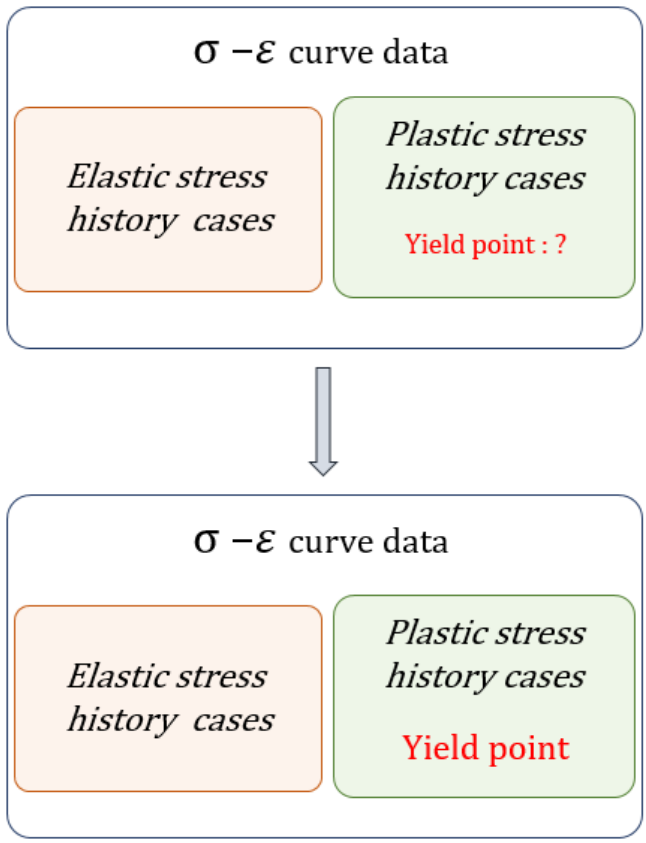

Figure 4.2 The second step of the Data-processing; (a) Flowchart to capture yield points (b) schematic diagram to discover initial yield points

4.2. Symbolic Regression by Genetic Programming

The genetic program (GP) called GPTIPS [34], which is implemented in MATLAB, is capable of regressing symbolic equations by relating between input and output data. For effective learning of the GP, data preparation process was necessary. Two groups of dataset are prepared; one group is based on the initial yield

stresses from all the reference simulations while the other group is stemmed from the initial yield stresses from all SELIFE. All initial yield stresses are obtained from the proposed Data-processing. The two GP-driven yield criterion are visualized by using fimplicit3 function in MATLAB. Furthermore, comparison of Hill's anisotropic yield surface with the GP-driven yield surface is included to verify the feasibility of the GP-driven yield surface. Finally, the GP-driven yield criterion will be verified by conducting simulations with different material orientation.

Anisotropic constant parameters ($F, G, H,$ and N) from the Hill's 48 anisotropic yield criterion are necessary to express anisotropic plastic characteristics. Experimental specimen tests should take several times in order to obtain accurate $F, G, H,$ and N values since the anisotropic characteristics are significantly different depending on material properties and the material orientations, that is, $F, G, H,$ and N strongly depend on material properties.

The proposed methodology using the GP, however, has strong advantages of formulating anisotropic yield criterion without $F, G, H,$ and N constants from experimental tests. The GP can produce

proper constants only by relating between the input data and the output data. Those data are based on the data-processed initial yield stresses and the given initial yield stress. In general GP relation for anisotropic yield criterion can be defined as :

$$\sigma_{12}^2 = f(\sigma_{yo}^2, \sigma_{22}^2, \sigma_{11}^2, (\sigma_{11}\text{-}\sigma_{22})^2) \quad (7)$$

σ_{yo}^2 indicates the initial yield stress of the given material and σ_{ij}^2 indicates the data-processed initial yield stresses. As seen equation (7), $F, G, H,$ and N values were not involved in the general GP relation.

5. Verification of SELIFE and Self-Learning Data-Driven Yield Criterion

5.1. Verification of SELIFE from the Uniaxial Tensile Experimental Measurements

Before the demonstration of the proposed methodology, SELIFE simulation with experimental measurements is verified. The SELIFE simulation is conducted with the uniaxial tensile experimental measurements of flat specimen [35]. Force−displacement data were extracted by digitizer program and applied to SELIFE simulation. To examine only initial yield stress behavior, specific displacement interval raining from 0.00[mm] to 0.25[mm] was only accepted and the force−displacement measurements were interpolated within the interval. Total 11 pairs of force−displacement data were used for SELIFE simulation. The detail image of the force−displacement data is shown in Figure 5.1. The given equation (8) is ANN structure which was used for SELIFE simulation. Plane stress condition was assumed and reduced integration scheme was accepted to demonstrate uniaxial tensile simulation.

$$\sigma_n = \sigma_{NN}([\varepsilon_n, \varepsilon_{n-1}, \sigma_{n-1}, \varsigma_n]: [12 - 25 - 25 - 3]) \quad \textbf{(8)}$$

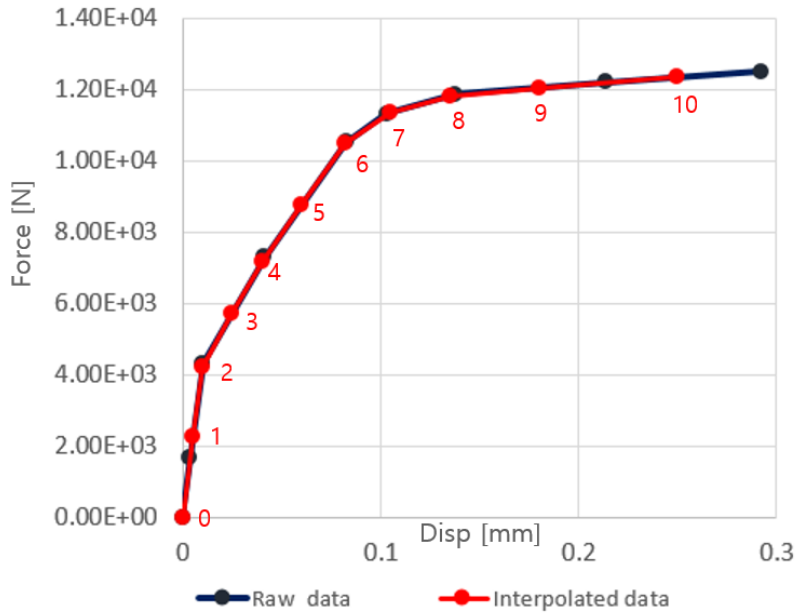

Figure 5.1 Interpolated force-displacement measurement for SELIFE simulation

SELIFE simulation was conducted with parameters shown in Table 5-1. Total 10 NN passes were used for the SELIFE but 5 NN passes are sufficient to extract reasonable force-displacement data. The results of the SELIFE simulation is shown in Figure 5.2. There is not dramatic change after the 3rd pass.

Table 5-1 Parameters for SELIFE simulations

Number of NN pass	Number of elements for train	Displacement error tolerance	NN epochs for pre-training	NN epochs for auto-adaptive training
10	264	0.03	1000	60

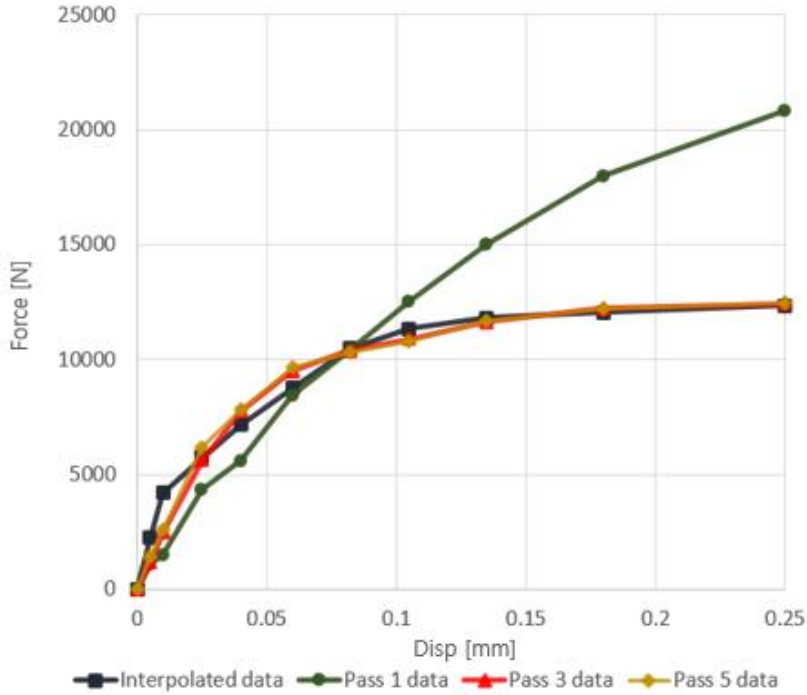

Figure 5.2 Force-displacement results of the SELIFE simulation by NN passes

Based on the stress-strain curves, the Data-processing was executed to capture the initial yield stress points. The points were positioned on the Von Mises surface. The material of the model is 2024-T351 aluminum alloy [35] and its initial yield stress is 330 [Mpa]. The data-processed initial yield stress points properly reflect on the tendency of the uniaxial tensile test. The plotted initial yield stresses are illustrated in Figure 5.3. The stress-strain data are from the results of the 5^{th} NN pass.

(a)

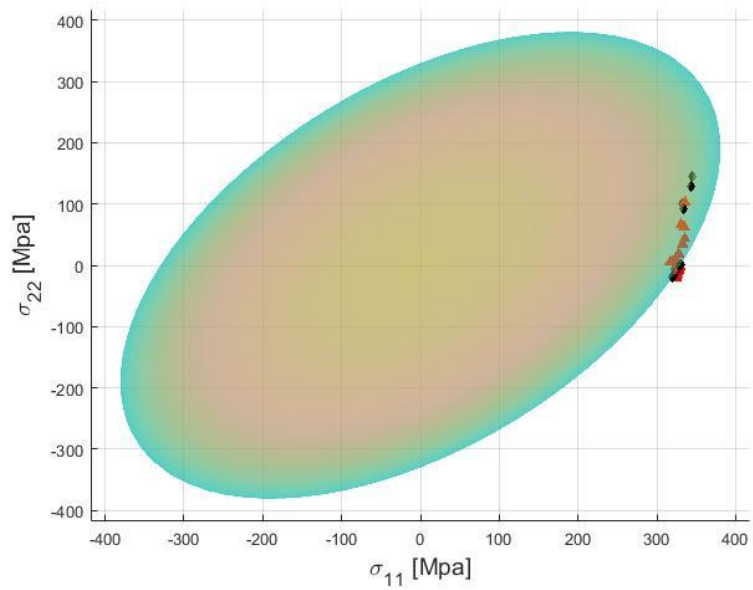

(b)

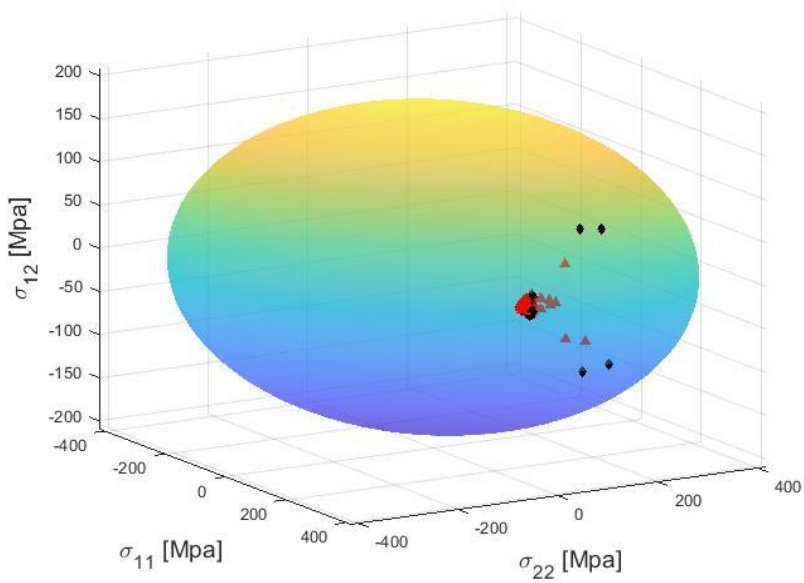

Figure 5.3 Data-processed initial yield stresses which are located on the Von Mises surface

The difference is defined as equation (9).

$$\sqrt{(\sigma_{11}^{y})^2 - (\sigma_{11}^{y}\sigma_{22}^{y}) + (\sigma_{22}^{y})^2 + 3\sigma_{12}^{y\,2}} - \sigma_{y0} = Difference \quad \textbf{(9)}$$

Based on this, all data-processed initial yield stresses are put into the Von Mises yield criterion to check the distribution of the difference. 1.4% of the average error was obtained. The detail image of the difference distribution is shown in Figure 5.4.

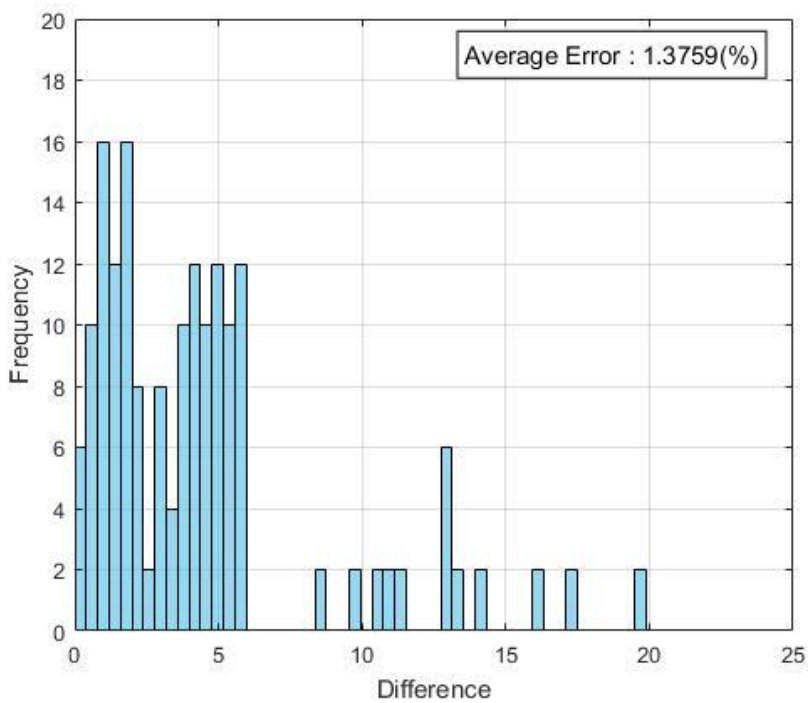

Figure 5.4 Distribution of numerical difference

5.2. Experimental Reference Simulations with Anisotropic Material

In addition to the isotropic material, in this section, anisotropic material is used for SELIFE simulations. In contrast with the previous section, reference simulations with anisotropic material were necessary to verify some results from SELIFE simulations by comparing force-displacement curves and stress-strain curves. In order to demonstrate reference simulations, a biaxial specimen made of anisotropic material with zero degree material orientation was chosen and simulated under several boundary conditions. Detail image for the biaxial specimen including some specific regions is shown in Figure 5.5. Four types of displacement boundary conditions (DBC) were defined to obtain sufficient initial yield stress in various stress states. 0.01mm magnitude for displacement was applied in Region A and B. The DBCs are arranged in Table 5-2. Fixed boundary conditions, however, were defined for the Region C and D. For stress-strain data extraction, the Region E was defined but sub-region of it was considered to save compute time of SELIFE. Furthermore, the sub-region of the Region E brought advantage for

balance between plastic stress history and elastic history within whole dataset. Specific elements where plasticity is likely to occur easily were set as the sub-region of the Region E. Total 220 elements for the sub-region, which are about 86% out of the Region E, were picked. Stress and strain dataset were extracted from the sub-region by using ABAQUS Python codes after each of the two ANN-based FEM i.e. FEM-A and FEM-B. The biaxial specimen was modeled in ABAQUS with material properties [36] shown in Table 5-3. For the experimental reference simulations, Hill's 48 anisotropic yield criterion was accepted. In addition, 2D plane stress condition was assumed for all reference simulations as well as SELIFE since the biaxial specimen assumed that it has the relatively small length in z-direction than the other directions (x and y-direction).

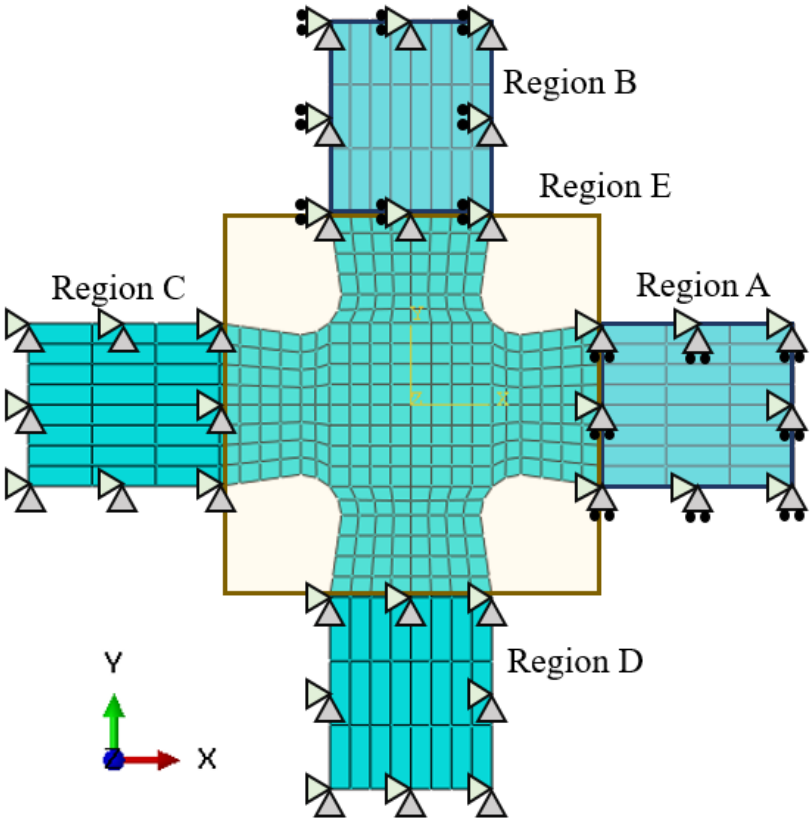

Figure 5.5 Boundary conditions for the biaxial specimen; Region A and B for the displacement boundary conditions; Region C and D for the fixed boundary conditions; Region E (256 elements) for data extraction

Table 5-2 Four types of displacement boundary conditions

Boundary types	Region A	Region B
Type 1	Tension	Tension
Type 2	Compression	Compression
Type 3	Compression	Tension
Type 4	Tension	Compression

Table 5-3 Material properties of anisotropic metal (DDQ mild steel [36])

Young's modulus, E [GPa]	206
Poisson's ratio, ν	0.3
Initial yield stress, σ_{y0} [MPa]	152.0
Lankford ratios : r_0, r_{45}, r_{90}	2.64, 1.57, 2.17
State of anisotropy of the material	

Hill' s 48 anisotropic yield criterion [37] was accepted to demonstrate anisotropic behavior of the material and the equation is defined as follows:

$$f(\sigma) = \sqrt{F(\sigma_{22}-\sigma_{33})^2 + G(\sigma_{33}-\sigma_{11})^2 + H(\sigma_{11}-\sigma_{22})^2 + 2L{\sigma_{23}}^2 + 2M{\sigma_{31}}^2 + 2N{\sigma_{12}}^2} \quad \textbf{(10)}$$

σ_{ij} are the stress components and $F, G, H, L, M,$ and N are constants parameters that express current state of anisotropic behavior. They can be defined as using combinations of yield stress ratio R_{ij} or using measured yields stress $\bar{\sigma}_{y0}$ and the material yield stress σ_{y0}.

$$\mathrm{F} = \frac{\sigma_{y0}}{2}\left(\frac{1}{\bar{\sigma}_{22}^2} + \frac{1}{\bar{\sigma}_{33}^2} - \frac{1}{\bar{\sigma}_{11}^2}\right) = \frac{1}{2}\left(\frac{1}{{R_{22}}^2} + \frac{1}{{R_{33}}^2} - \frac{1}{{R_{11}}^2}\right)$$

$$\mathrm{G} = \frac{\sigma_{y0}}{2}\left(\frac{1}{\bar{\sigma}_{33}^2} + \frac{1}{\bar{\sigma}_{11}^2} - \frac{1}{\bar{\sigma}_{22}^2}\right) = \frac{1}{2}\left(\frac{1}{{R_{33}}^2} + \frac{1}{{R_{11}}^2} - \frac{1}{{R_{22}}^2}\right)$$

$$\mathrm{H} = \frac{\sigma_{y0}}{2}\left(\frac{1}{\bar{\sigma}_{11}^2} + \frac{1}{\bar{\sigma}_{22}^2} - \frac{1}{\bar{\sigma}_{33}^2}\right) = \frac{1}{2}\left(\frac{1}{{R_{11}}^2} + \frac{1}{{R_{22}}^2} - \frac{1}{{R_{33}}^2}\right)$$

$$\mathrm{L} = \frac{3}{2}\left(\frac{\sigma_{y0}^2}{\sqrt{3}}\frac{1}{\bar{\sigma}_{23}^2}\right) = \frac{3}{2}\left(\frac{\tau_{y0}^2}{\bar{\sigma}_{23}^2}\right) = \frac{3}{2{R_{23}}^2}$$

$$M = \frac{3}{2}\left(\frac{\sigma_{y0}^2}{\sqrt{3}}\frac{1}{\bar{\sigma}_{13}^2}\right) = \frac{3}{2}\left(\frac{\tau_{y0}^2}{\bar{\sigma}_{13}^2}\right) = \frac{3}{2{R_{13}}^2}$$

$$N = \frac{3}{2}\left(\frac{\sigma_{y0}^2}{\sqrt{3}}\frac{1}{\bar{\sigma}_{12}^2}\right) = \frac{3}{2}\left(\frac{\tau_{y0}^2}{\bar{\sigma}_{12}^2}\right) = \frac{3}{2{R_{12}}^2} \quad \textbf{(11)}$$

As seen equation (11), yield stress ratios R_{ij} are defined as the ratio of the measured yield stress $\bar{\sigma}_{ij}$ to material initial yield stress σ_{y0}.

$$R_{ij} = \frac{\bar{\sigma}_{ij}}{\sigma_{y0}} \text{ (for } ij \text{ =11, 22, and 33)}$$

$$R_{ij} = \frac{\bar{\sigma}_{ij}}{\tau_{y0}} \text{ (for } ij \text{ =12, 13, and 23)} \quad \textbf{(12)}$$

$$\text{where } \tau_{y0} = \frac{\sigma_{y0}}{\sqrt{3}}$$

ABAQUS anisotropic simulations are taken into account using only yield stress ratios R_{ij}.Since the plane stress condition was applied to all simulations, it is convenient to assume R_{ij} as following [15, 38]. The 22, 33, and 12 components of yield stress ratios can be defined in terms of the Lankford ratios.

$$R_{11} = R_{13} = R_{23} = 1$$

$$R_{22} = \sqrt{\frac{r_{90}(r_0+1)}{r_0(r_{90}+1)}},\ R_{33} = \sqrt{\frac{r_{90}(r_0+1)}{r_0+r_{90}}},\ R_{12} = \sqrt{\frac{3r_{90}(r_0+1)}{(2r_0+1)(r_0+r_{90})}} \quad \textbf{(13)}$$

Moreover, equation (10) can be reduced by equation (14).

Thus, $F, G, H,$ and N are only necessary to complete equation (14).

$$f(\sigma) = \sqrt{F\sigma_{22}^2 + G\sigma_{11}^2 + H(\sigma_{11} - \sigma_{22})^2 + 2N\sigma_{12}^2} \quad \textbf{(14)}$$

Therefore, the following yield criterion is used for the anisotropic yield simulations based on equation (14).

$\sqrt{F\sigma_{22}^2 + G\sigma_{11}^2 + H(\sigma_{11} - \sigma_{22})^2 + 2N\sigma_{12}^2} - \sigma_{y0} < 0$: Elastic deformation **(15)**

$\sqrt{F\sigma_{22}^2 + G\sigma_{11}^2 + H(\sigma_{11} - \sigma_{22})^2 + 2N\sigma_{12}^2} - \sigma_{y0} = 0$: Plastic deformation **(16)**

Equation (16) is, in particularly, converted to equation (17), which is Hill' s 48 anisotropic yield criterion.

$$F\sigma_{22}^2 + G\sigma_{11}^2 + H(\sigma_{11} - \sigma_{22})^2 + 2N\sigma_{12}^2 = \sigma_{y0}^2 \quad \textbf{(17)}$$

By using Lankford values in Table 5-3 and (13), the yield stress ratios can be obtained. Then, based on equation (17), the elliptic shape for anisotropic yield surface could be displayed in the stress space $\{\sigma_{11}, \sigma_{22},$ and, $\sigma_{12}\}$. The image of the yield surface is shown in Figure 5.6

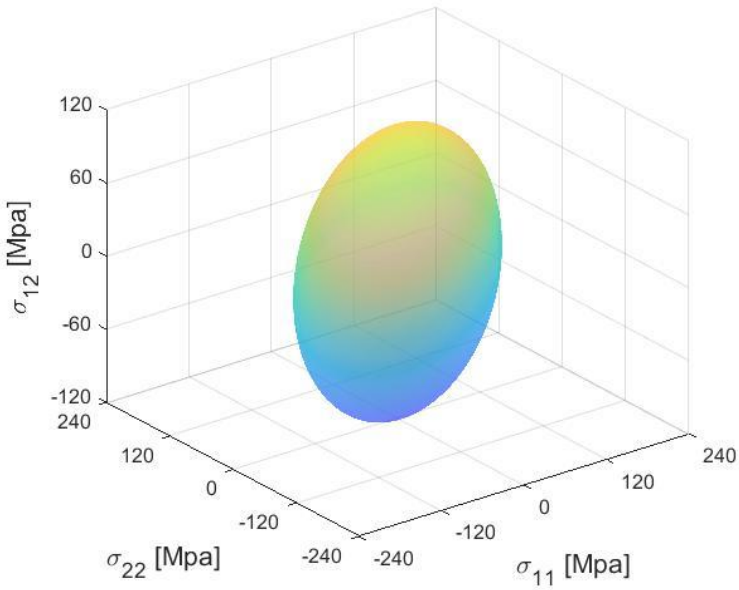

Figure 5.6 Hill's 48 anisotropic yield surface under the plane stress condition

The intersections between the yield surface and the each of axes are the measured yield stresses. This relation will be used for the verification of GP driven anisotropic equations. By putting $\sigma_{22} = \sigma_{12} = 0$ in equation (17), the 11 component of the measured yield stress can be obtained.

$$(G + H)\sigma_{11}^2 = \sigma_{y0}^2 \quad \textbf{(18)}$$

$$\sigma_{11}^2 = \frac{\sigma_{y0}^2}{(G + H)} \quad \textbf{(19)}$$

$$\sigma_{11} = \pm\frac{\sigma_{y0}}{\sqrt{G + H}} = \pm\sigma_{y0}\, R_{11} = \pm\bar{\sigma}_{11} \quad \textbf{(20)}$$

Similarly, the 22 component of the measured yield stress can be computed.

$$\boldsymbol{\sigma_{22} = \pm\frac{\sigma_{y0}}{\sqrt{F+H}} = \pm\sigma_{y0}\, R_{22} = \pm\bar{\sigma}_{22}} \quad \textbf{(21)}$$

The measured yield stress for the 12 component can be calculated from the similar approach.

$$2N\sigma_{12}^2 = \sigma_{y0}^2 \quad \textbf{(22)}$$

$$\sigma_{12}^2 = \frac{\sigma_{y0}^2}{2N} \quad \textbf{(23)}$$

$$\sigma_{12} = \pm\frac{\sigma_{y0}}{\sqrt{2N}} = \pm\frac{\sigma_{y0}}{\sqrt{3}}R_{12} = \pm\frac{\sigma_{y0}}{\sqrt{3}}\frac{\bar{\sigma}_{12}}{\tau_{y0}} = \pm\bar{\sigma}_{12} \quad \textbf{(24)}$$

Therefore, measured yield stresses can be achieved based on equation (20), (21), and (24). Both yield stress ratios measured yield stresses are arranged by the each of the components in Table 5-4. In addition to using equation (20), (21), and (24), the intersection points were numerically calculated by finding the points which are minimum distance between the surface and axes. In order to show the obtained intersection values, those values are displayed with the Hill's 48 anisotropic yield surface in Figure 5.7. The same values of the measured yield stresses could be achieved.

Table 5-4 Calculated yield stress ratios and measured yield stress

Components	Yield stress ratios	Measured yield stresses [Mpa]
11 component	$R_{11} = 1.0000$	$\bar{\sigma}_{11} = \pm 152$
22 component	$R_{22} = 0.9715$	$\bar{\sigma}_{22} = \pm 147.6680$
12 component	$R_{12} = 1.0909$	$\bar{\sigma}_{12} = \pm 95.7344$

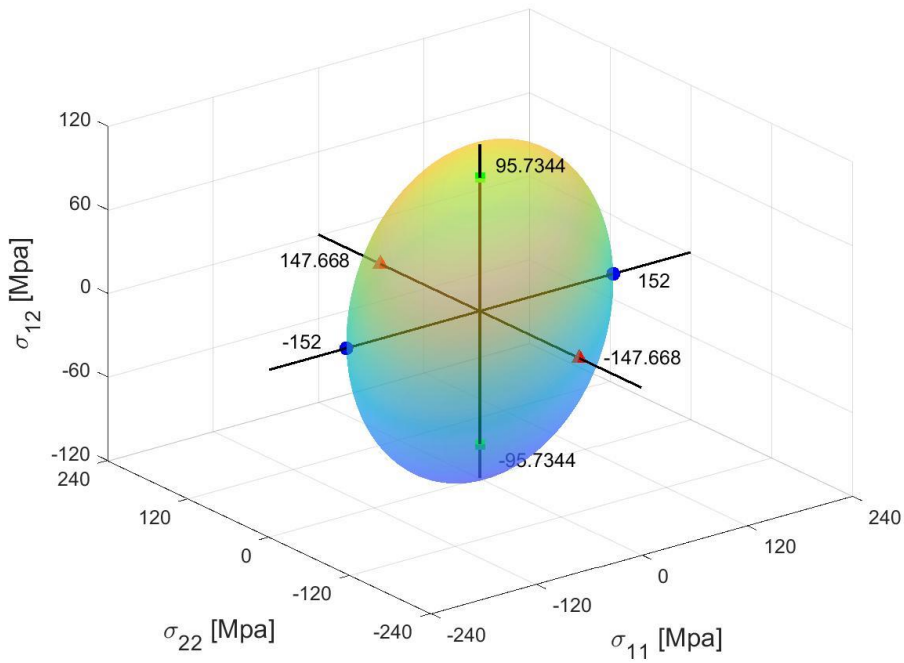

Figure 5.7 Hill's 48 anisotropic yield surface with intersections

To verify anisotropic yield response, the reference simulation with boundary type 1 was investigated. The resultant force-displacement curve is shown in Figure 5.8(a). The forces from both the Region A and B change differently after the specific point due to Hill's anisotropic yield criterion. Figure 5.8 (b) is force-displacement curve from simulation with Von Mises yield criterion. Forces from both the Region A and B are no difference after specific point.

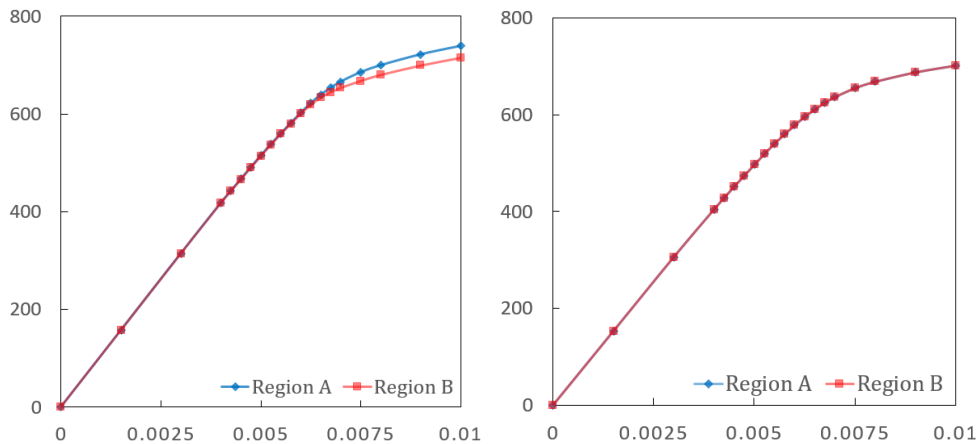

Figure 5.8 Force-displacement curves from (a) Hill's anisotropic yield criterion and (b) Von Mises yield criterion

As mentioned earlier, all experimental boundary measurements i.e. global reaction forces, displacements, and

internal displacements were substituted with the FE reference simulations of experiment.

5.3. ANN Architecture and Self-Learning Parameters

SELIFE simulations were performed with all four boundary types individually. Twelve input nodes were required to learn stress, strain, and internal variable data and three output nodes to predict stress data. In addition, thirty hidden nodes of the ANN were chosen as an experiment. The same ANN architecture shown in equation (25) was used for all SELIFE.

$$\sigma_n = \sigma_{NN}([\varepsilon_n, \varepsilon_{n-1}, \sigma_{n-1}, \varsigma_n]: [12 - 30 - 30 - 3]) \qquad (25)$$

SELIFE simulations from the each of the boundary types were conducted with the proposed parameters which are arranged in Table 5-5. Based on the proposed ANN architecture and SELIFE parameters, the results of the SELIFE with boundary type1 (Tension-Tension DBC) will be shown in the next section.

Table 5-5 Parameters for SELIFE simulations

Displacement Boundary type	Number of NN pass	Number of elements for train	Displacement error tolerance	NN epochs for pre-training	NN epochs for autop training
Type 1 (T-T)	8	220	0.01	1000	70
Type 2 (C-C)	8	220	0.01	1000	70

Type 3 (C-T)	5	220	0.015	1000	90
Type 4 (T-C)	5	220	0.015	1000	90

5.4. Results from SELIFE Simulation with Tension-Tension Displacement Boundary Condition

In order to illustrate plastic area in Region E, an effective plastic strain contour based on the reference simulation with tension-tension displacement boundary condition (the boundary type 1) are added in Figure 5.9. The image is from the last analysis step. Two specific elements were chosen to examine stress-strain history curves. One is from the 138th element which has elastic characteristic. On the other hand, the 132nd element shows plastic behavior. From the each element, stress-strain curves are plotted together to show the update of ANN-based constitutive model during the multiple SELIFE NN passes.

Figure 5.10 and Figure 5.11 illustrate the global responses of the biaxial specimen by SELIFE NN passes. Figure 5.10 explains the global responses from the Region A. Reaction force-displacement curves in x-direction are shown in Figure 5.10 (a) while reaction force history in the y-direction and reaction moment history are

shown in Figure 5.10 (b) and Figure 5.10 (c), respectively. Since the Region A can move only in x−direction but fixed in y−direction, only force−displacement curve in x−direction could be obtained. Because of material anisotropy and effects of deformation in the other direction, reaction moment was occurred during the SELIFE.

On the other hand, Figure 5.11 account the global responses from the Region B. Force−displacement curves in the y−direction are included in Figure 5.11 (b). Reaction force history in x direction and reaction moment history are depicted in Figure 5.11 (a) and Figure 5.11 (c), respectively. As seen the change of the global responses by SELIFE NN passes from Figure 5.10 and Figure 5.11, all curves approach their target curves as NN pass increasing.

For stress contour comparison, Figure 5.12, Figure 5.13, and Figure 5.14 are also included. Comparing with the results from the reference simulation, SELIFE was capable of producing similar stress contours.

In order to verify the effect of multiple NN passes, stress−strain curves were investigated as well. The plastic behavior of the 132nd element could be updated by repetitive NN passes as seen Figure

5.15. Similarly, in Figure 5.16, the elastic stress history from the 138th element was able to be revised by the iterative stress−strain training. As the NN pass increasing, the accuracy of stresses tended to improve. The ANN−based constitutive model allows the FE model of the SELIFE to demonstrate complex material behavior based on trained data. As seen Figure 5.15 and Figure 5.16, SELIFE is able to learn stress data regardless of material behavior. Similar update by the several SELIFE NN passes also appeared in the other SELIFE.

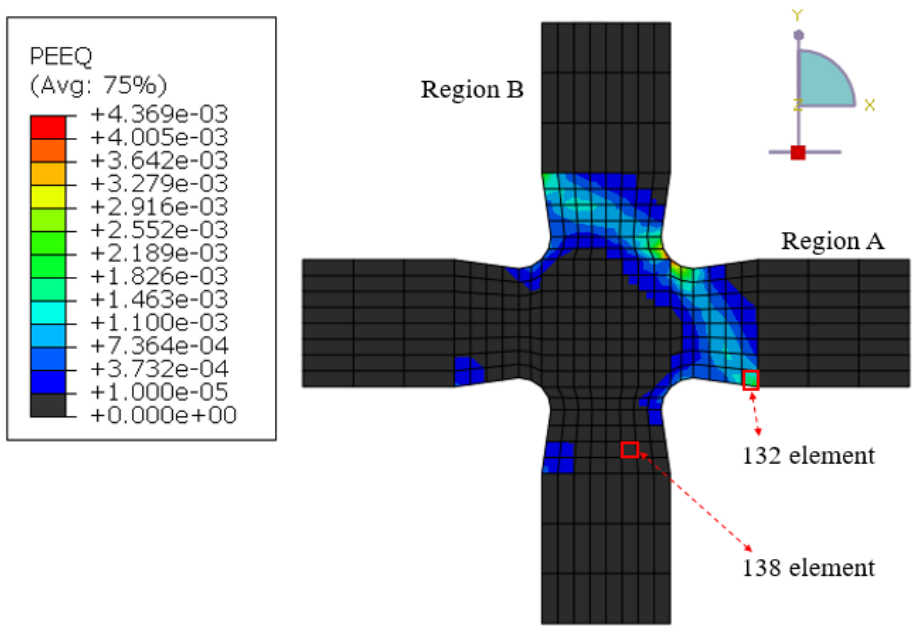

Figure 5.9 Effective plastic strain contour from the reference simulation under tension-tension displacement boundary condition (boundary type 1)

(a)

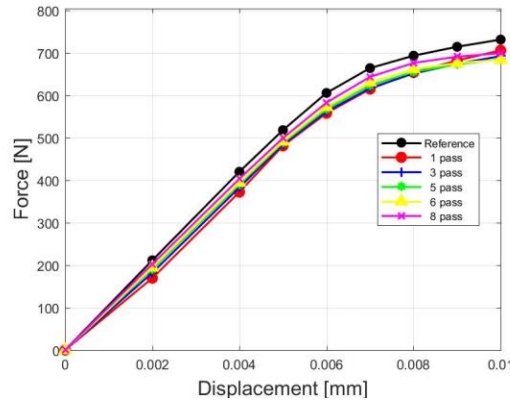

(b)

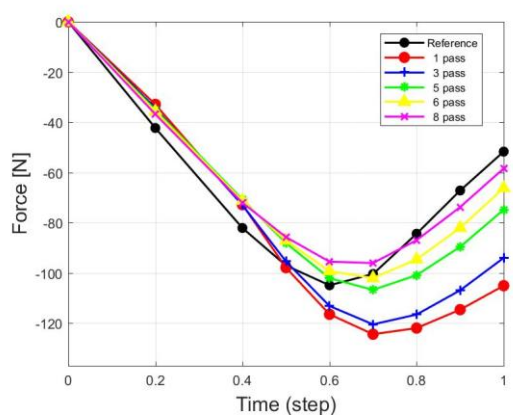

(c)

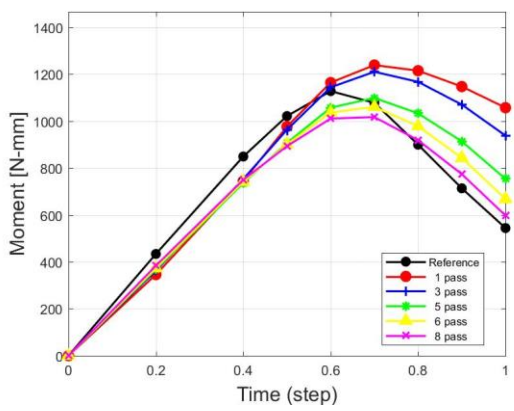

Figure 5.10 Curves from the Region A by SELIFE NN passes; (a) reaction force-displacement curve in x direction, (b) reaction force history curve in y direction, and (c) reaction moment history curve

(a)

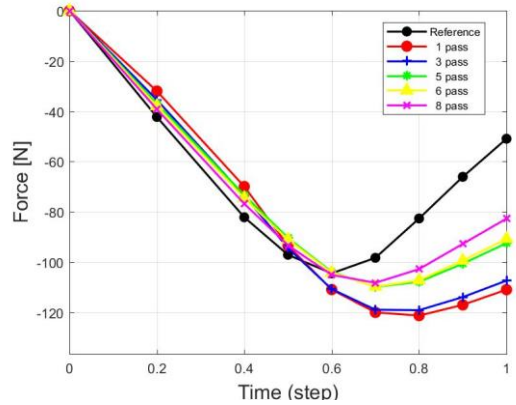

(b)

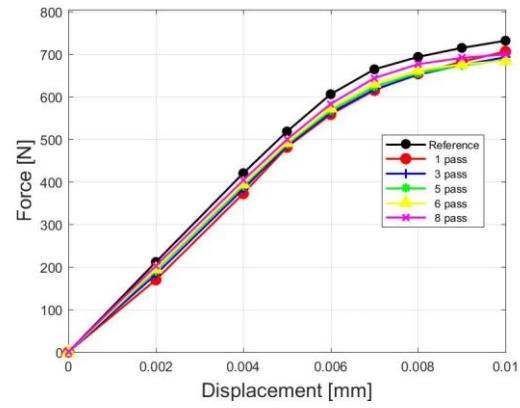

(c)

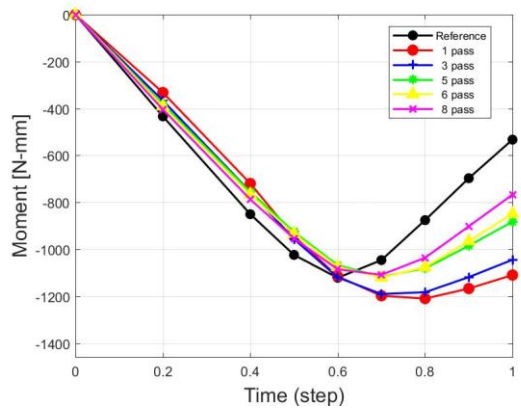

Figure 5.11 Curves from the Region B by SELIFE NN passes; (a) reaction force history curve in x direction, (b) reaction force-displacement curve in y direction, and (c) reaction moment history curve

(a)

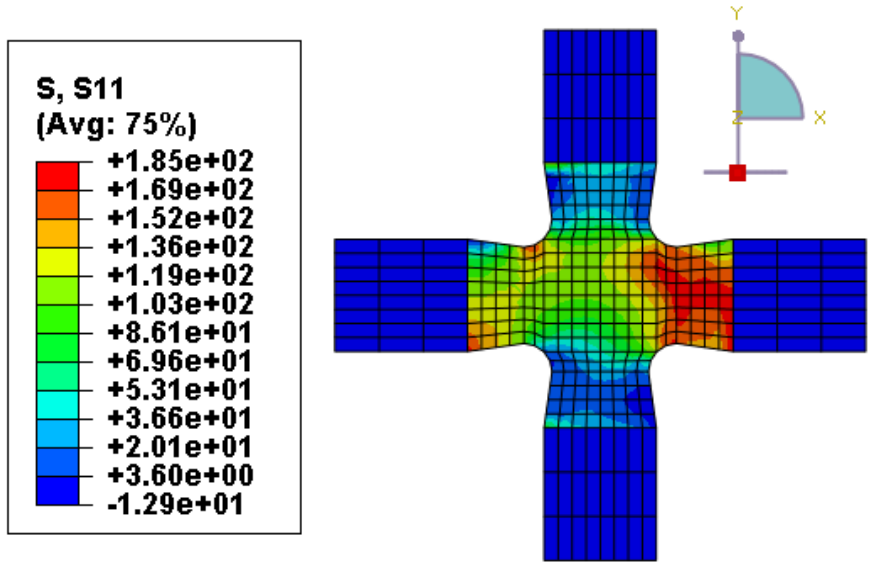

(b)

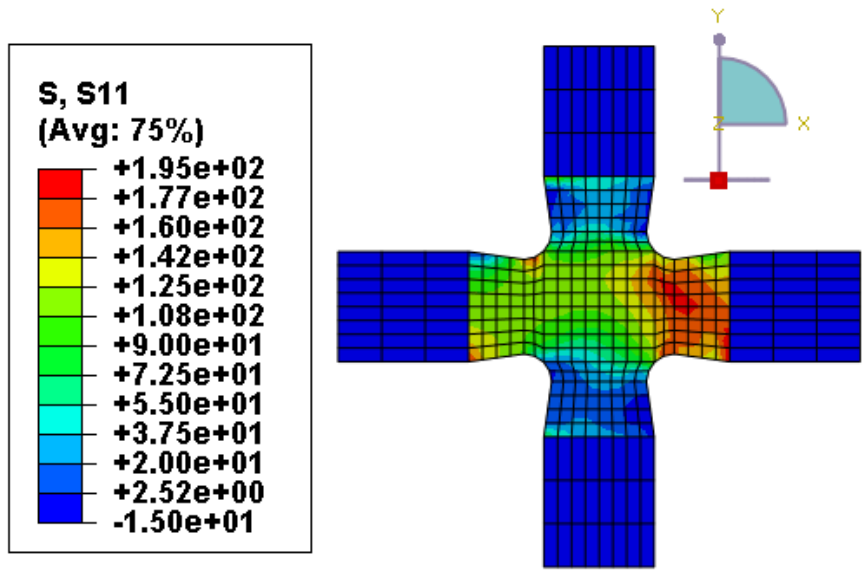

Figure 5.12 Stress (S11) contour comparison; (a) result of the reference simulation and (b) result of SELIFE simulation at the last pass (the 8th pass)

(a)

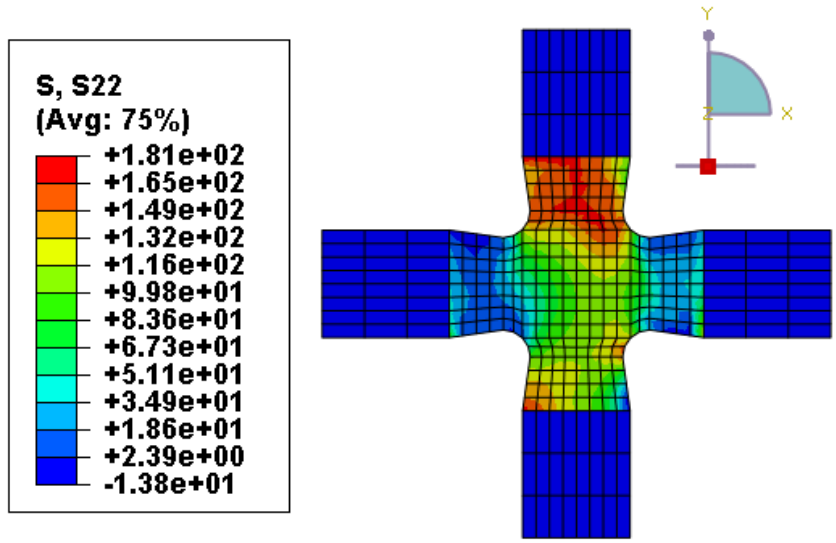

(b)

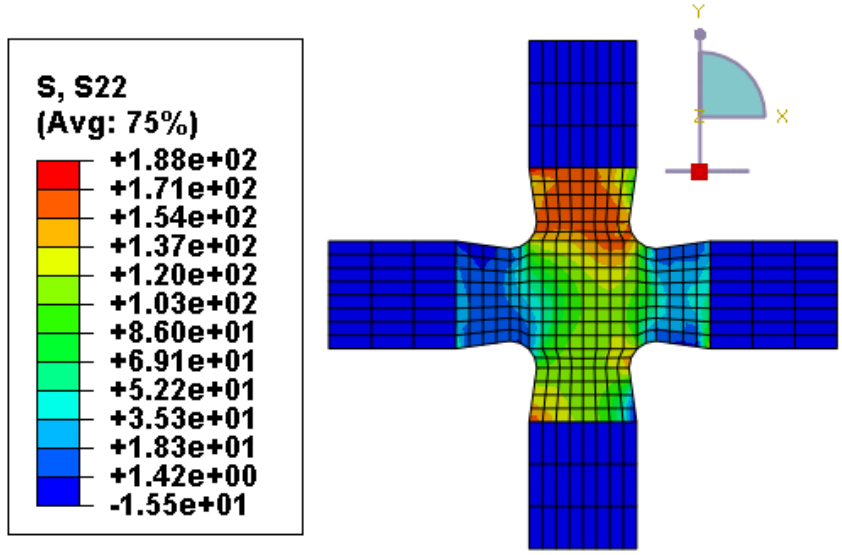

Figure 5.13 Stress (S22) contour comparison; (a) result of the reference simulation and (b) result of SELIFE simulation at the last pass (the 8th pass)

(a)

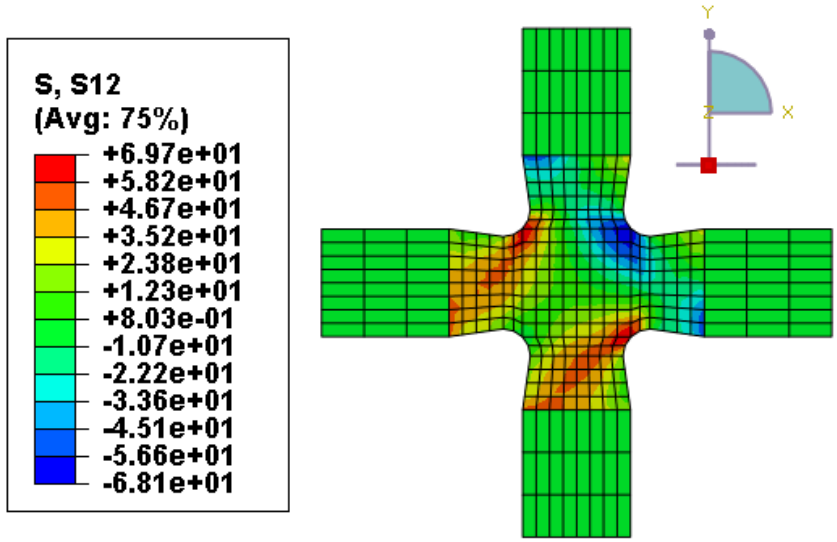

(b)

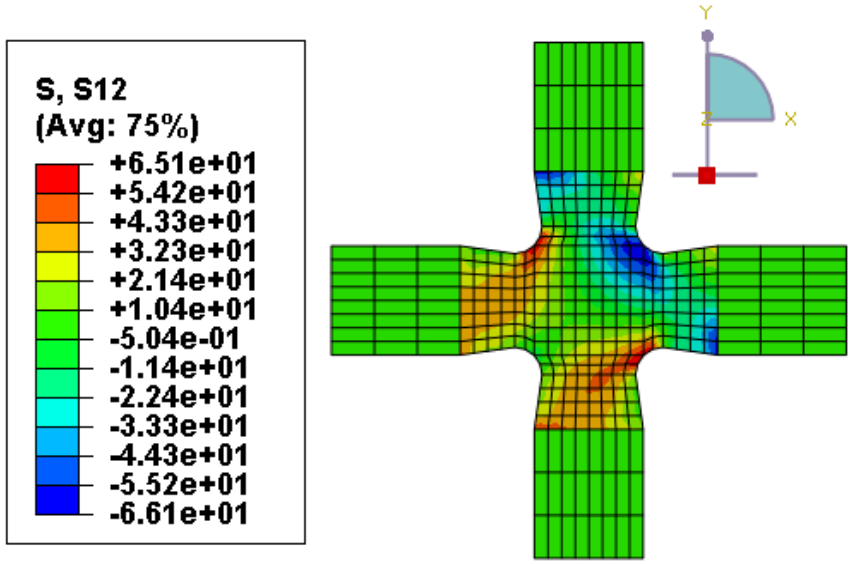

Figure 5.14 Stress (S12) contour comparison; (a) result of the reference simulation and (b) result of SELIFE simulation at the last pass (the 8th pass)

(a)

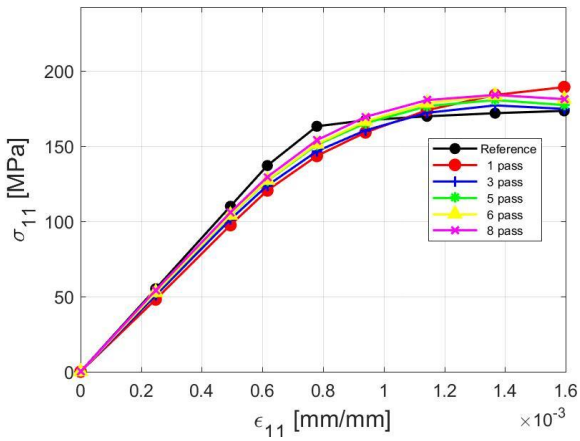

(b)

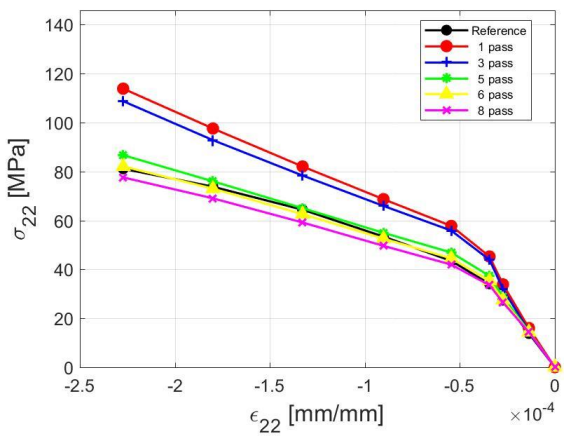

(c)

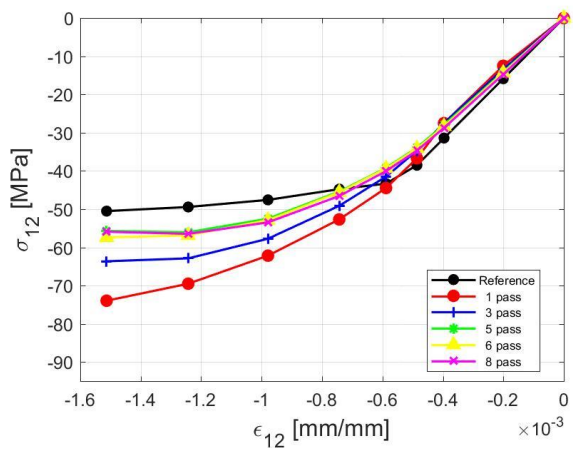

Figure 5.15 Stress-strain curves at the 3rd gauss point in the 132nd element by SELIFE NN passes

(a)

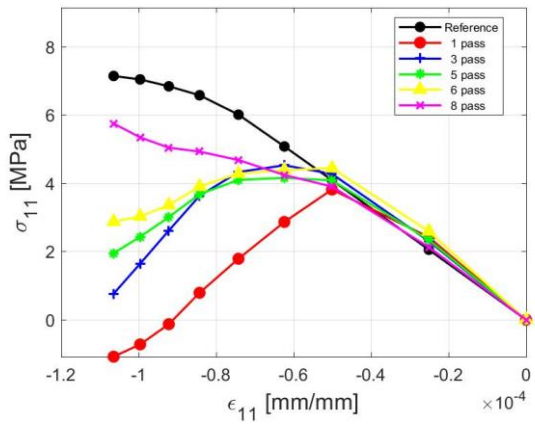

(b)

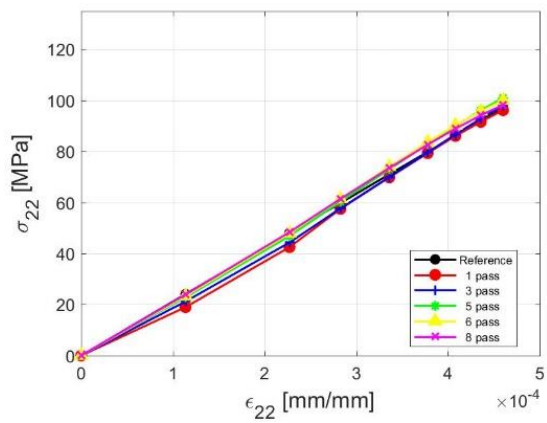

(c)

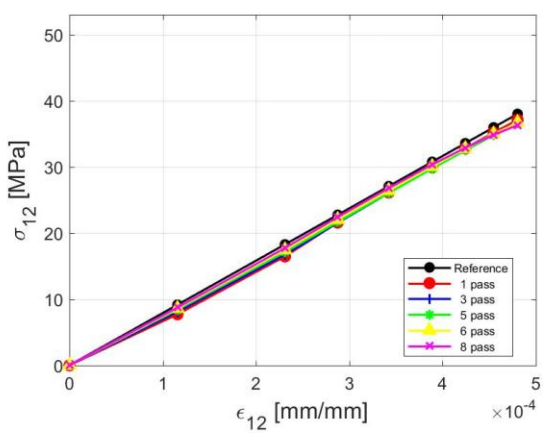

Figure 5.16 Stress-strain curves at the 2nd gauss point in the 138th element by SELIFE NN passes

5.5. Data-Processing

Stress-strain curves from the SELIFE with boundary type 1 were used to demonstrate the Data-processing algorithm. Two types of the initial yield stress are compared. One is calculated based on Hill's anisotropic yield criterion. The other is, however, obtained by Data-processing. The two yield stresses were plotted on the each of the same stress-strain curves in Figure 5.17. The three specific gauss points in the Region E were chosen to illustrate the comparison of the initial yield stress. The circle blue dots on the each of the stress-strain curves are the initial yield points satisfying Hill's 48 anisotropic yield criterion while the asterisk red dots are obtained from the Data-processing. Comparing with each two initial yield points on the each of the curves, the yield stresses obtained by the Data-processing were located at reasonable yield positions. The majority of the data-processed initial yield stresses was close to the initial yield stress satisfying Hill's anisotropic yield criterion.

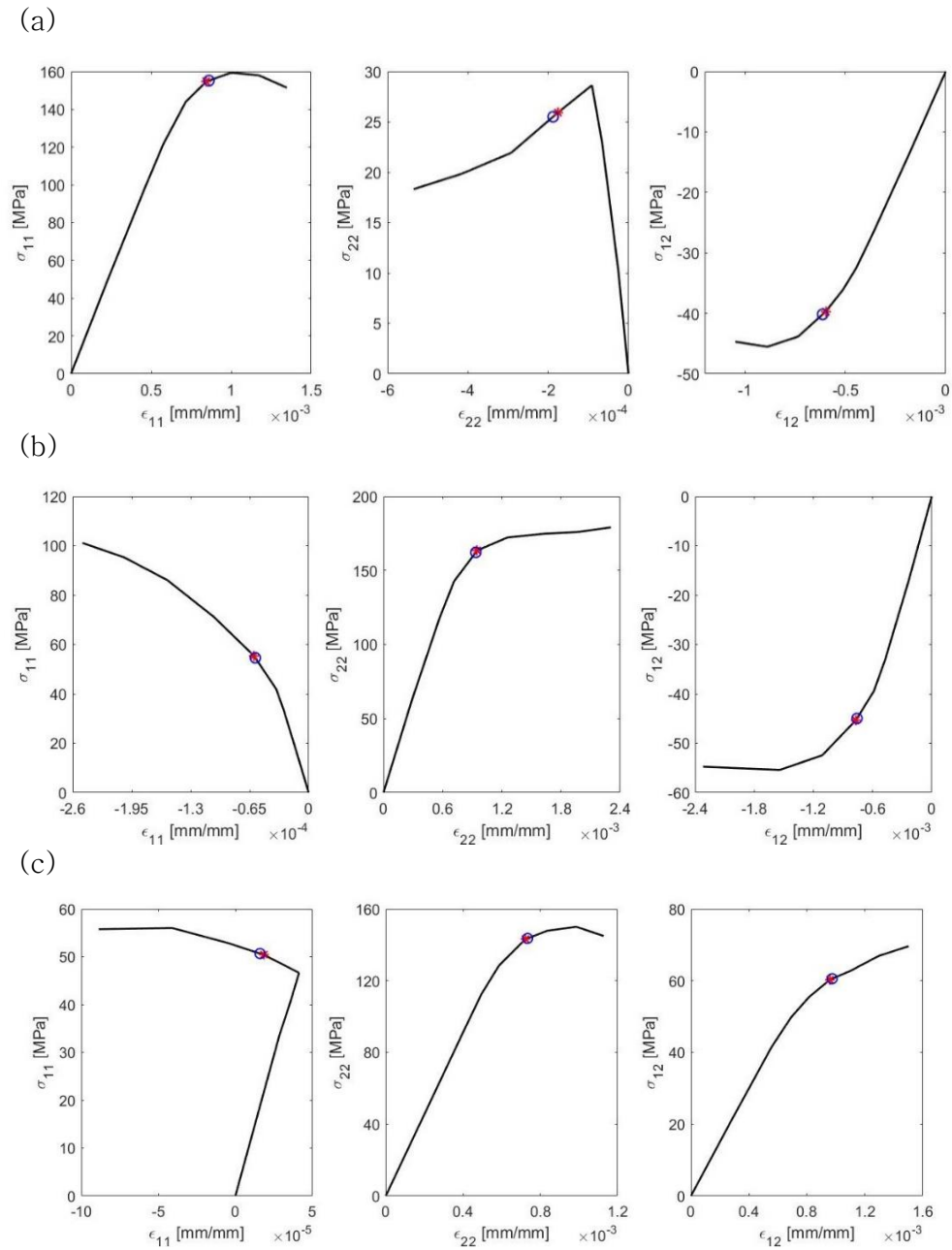

Figure 5.17 Comparison of the initial yield stress positions; (a) at the 2nd gauss point in the 131st element, (b) at the 2nd gauss point in the 184th element, and (c) at the 2nd gauss point in the 240th element

In order to verify the feasibility of the Data-processing, two groups of the initial yield stresses were set and the values were plotted on the Hill's anisotropic yield surface for appreciable comparison. The group one consisted of the data-processed initial yield stresses from all reference simulations and the other group contained the data-processed initial yield stresses from the self-learned stress-strain curves. Furthermore, all data-processed initial yield stress were put into the Hill's anisotropic yield criterion (14) to investigate the distribution of the numerical difference, that is, equation (26) was introduced to calculate the difference between Hill's anisotropic yield surface and the data-processed initial yield stresses. σ_{ij}^{y} indicates the discovered initial yield stresses by means of the Data-processing, σ_{y0} represents initial yield stress of the given material, and $F, G, H,$ and N are anisotropic parameters.

$$\sqrt{F\,{\sigma_{22}^{y}}^{2} + G\,{\sigma_{11}^{y}}^{2} + H\left(\sigma_{11}^{y} - \sigma_{22}^{y}\right)^{2} + 2N{\sigma_{12}^{y}}^{2}} - \sigma_{y0} = Difference \qquad \textbf{(26)}$$

Based on the data-processed initial yield stresses from the reference stress-strain data, the points were plotted on the anisotropic yields surface in Figure 5.18 (a). Moreover, the

histogram which shows the distribution of the difference between the initial yield stresses and Hill's anisotropic yield surface is included in Figure 5.18 (b). Most of the initial yield stresses are close to the yield surface and the average percent of the difference distribution is 0.9730 %. The proposed data-processing algorithm has reasonable to acquire the initial yield stresses from any stress-strain curves which includes the plastic behavior.

(a)

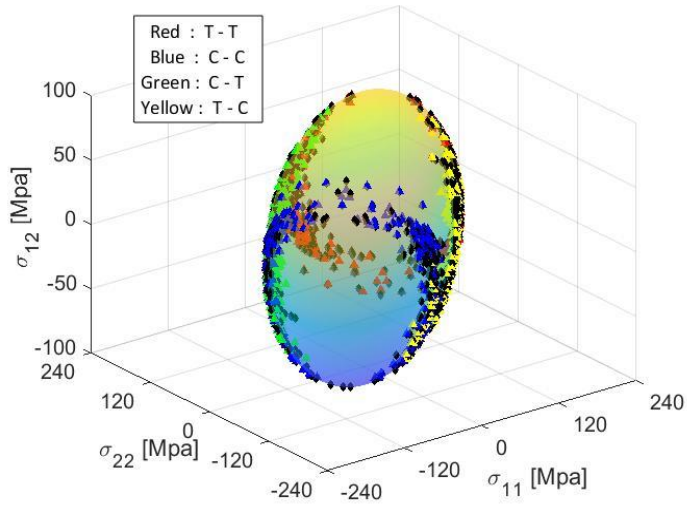

(b)

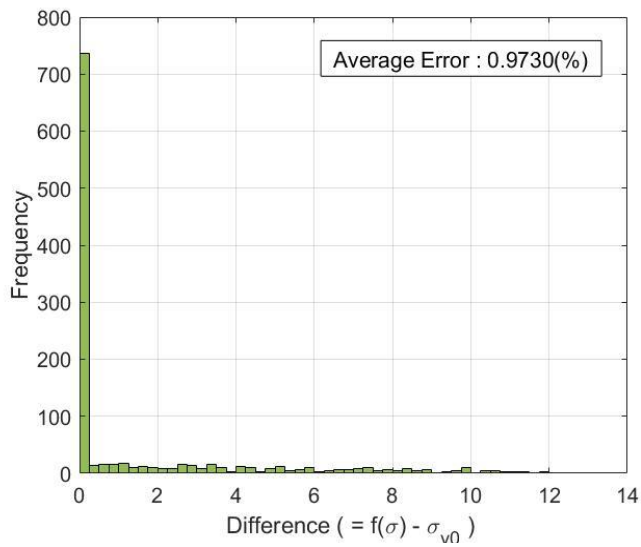

Figure 5.18 Investigation of data-processed initial yield stresses based on all reference simulations; (a) data-processed initial yield stresses on the Hill's yield surface, (b) distribution of numerical difference between data-processed initial yield stress and the Hill's anisotropic yield criterion

Note that the four colors were chosen to distinguish which boundary conditions caused the initial yield stress points. Red dots represent initial yield stresses from boundary type 1 (Tension-Tension DBC). Blue ones are from boundary type 2 (Compression-Compression DBC), Green from the boundary type 3 (Compression-Tension DBC), and Yellow from the boundary type 4 (Tension-Compression DBC), respectively. However, all black dots are the initial yield stresses satisfying the Hill's anisotropic yield criterion (17).

Similarly, the data-processed initial yield stresses based on the self-learned stress-strain data were plotted on the same yield surface. The results are shown in Figure 5.19 (a). The histogram to illustrate the distribution of the difference is depicted in Figure 5.19 (b). Average value of the difference distribution somewhat increased but most of the initial yield stresses are reasonably located on the Hill's anisotropic yield surface.

(a)

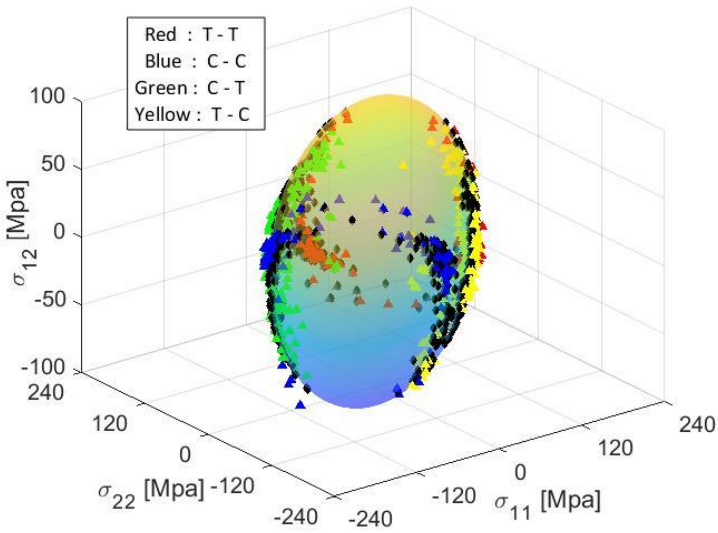

(b)

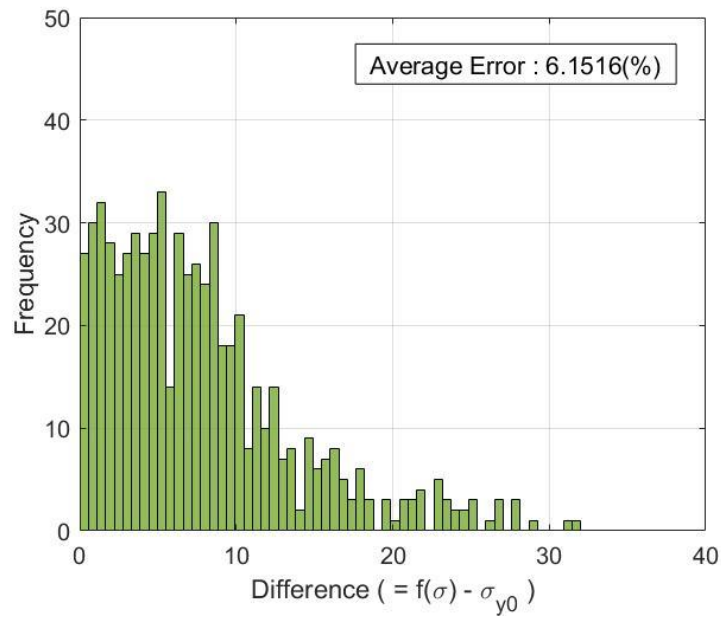

Figure 5.19 Investigation of data-processed initial yield stresses based on all SELIFE simulations; (a) data-processed initial yield stresses on the Hill's yield surface, (b) distribution of numerical difference between data-processed initial yield stress and the Hill's anisotropic yield criterion

5.6. Data Preparation for Genetic Programming

As aforementioned, the general GP relation for anisotropic yield criterion is able to be defined as (7). The inputs are combinations of quadratic terms of σ_{11}, σ_{22}, and σ_{yo}. On the other hand, for the output of the GP, σ_{12}^2 was chosen and arranged in ascending order for effective GP training. Corresponding input datasets were arranged as pairs of the output dataset. Input dataset and output dataset for the GP are arranged in Table 5-6.

Table 5-6 Input datasets and output dataset for the genetic program

Input datasets				Output dataset
$X1 = \sigma_{yo}^2$	$X2 = \sigma_{22}^2$	$X3 = \sigma_{11}^2$	$X4 = (\sigma_{11} - \sigma_{22})^2$	$Y1 = \sigma_{12}^2$
corresponding input data for minimum σ_{12}^2 value				Minimum ↓ (Ascending order) ↓
⋮				
corresponding input data for maximum σ_{12}^2 value				Maximum

The GP [34] requires both a training dataset and a test dataset. The former dataset is for learning a relationship between input and output while the latter dataset is to validate the relationship. The

training dataset was prepared from the data-processed initial yield stresses but the test dataset was based on initial yield stresses satisfying the Hill's 48 anisotropic yield equation (17). Both training and test dataset were arranged as following Table 5-6.

Several parameters affecting the results of the GP training are shown in Table 5-7 and the operational functions shown in Table 5-8 were activated to drive appreciable yield criterion. Two groups of the initial yield stress database were arranged as the proposed method depicted in Table 5-6 and trained under the same conditions as following Table 5-7 and Table 5-8.

Table 5-7 Parameters for genetic program

Parameter description	Value
Number of population size	50
Number of generation	50
Maximum number of genes per individual	3
Maximum depth for gene	5

Table 5-8 Activated functions for the genetic program

Activated function name	Symbols
Times	×
Minus	−
Plus	+

5.7. Self-Learning Data-Driven Anisotropic Yield Criterion from the Reference Simulations

First, the symbolic regression was conducted with the database based on the initial yield stresses captured from all the reference simulations by means of the data-processing. The data-driven anisotropic yield criterion is driven by the GP.

$$0.3126\sigma_{22}^2 + 0.2514\,\sigma_{11}^2 + 0.7566(\sigma_{11}-\sigma_{22})^2 + 2.8167\sigma_{12}^2 = \sigma_{yo}^2 \qquad (27)$$

Based on equation (27), the GP driven anisotropic yield surface is visualized by using the fimplicit3 function in MATLAB. To proper comparison, the Hill' s anisotropic yield surface is displayed together. Both anisotropic yield surfaces are shown in Figure 5.20. The blue surface is Hill' s anisotropic yield surface while the red one is stemmed from the GP driven criterion. In order to compare the results in more detail, yield surface images from both stress space (3D) and stress plane (2D) were included.

(a)

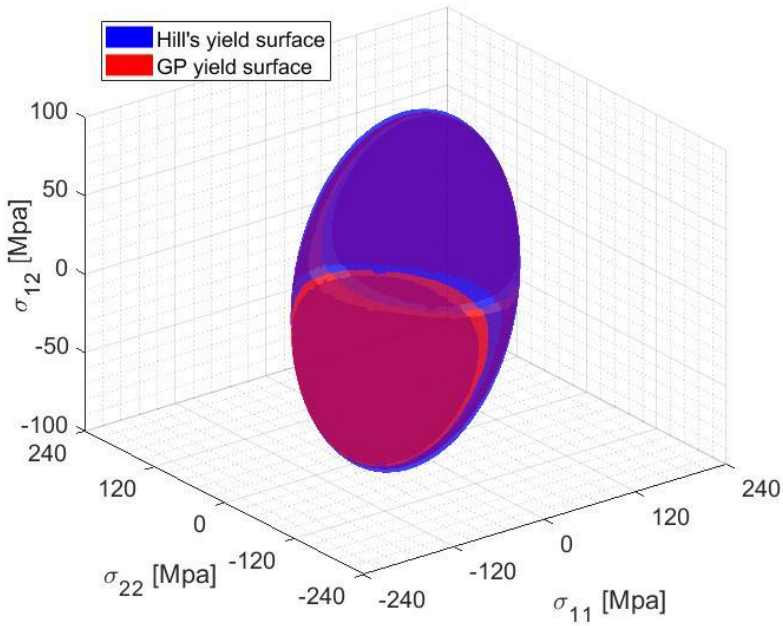

(b)

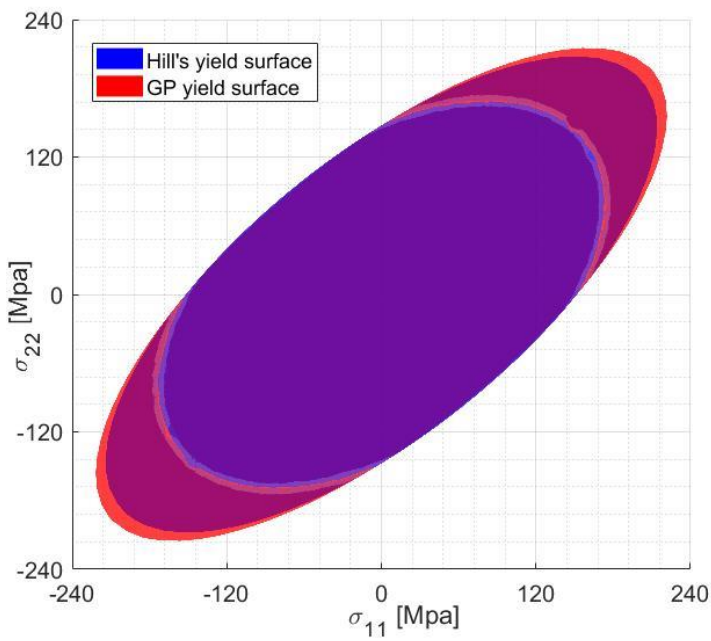

Figure 5.20 Comparison of anisotropic yield surfaces; (a) in the 3D stress space and (b) on the 2D stress plane

The prediction results from the GP are shown in Figure 5.21 (a) and (b). All upper graphs are from the results of training dataset while the bottom graphs are from those of test dataset. Figure 5.21 (a) illustrates the predictive performance by each of data. Furthermore, Figure 5.21 (b) indicates the relations between the predicted output values and actual output values. The closer the blue dots are to the linear line, the better the GP results can be expected. The accuracies of the training dataset and the test dataset are 94.2325% and 97.825%, respectively. Since the initial yield stresses which satisfies the Hill's 48 anisotropic yield criterion were used as the test dataset, the better performance was achieved.

(a)

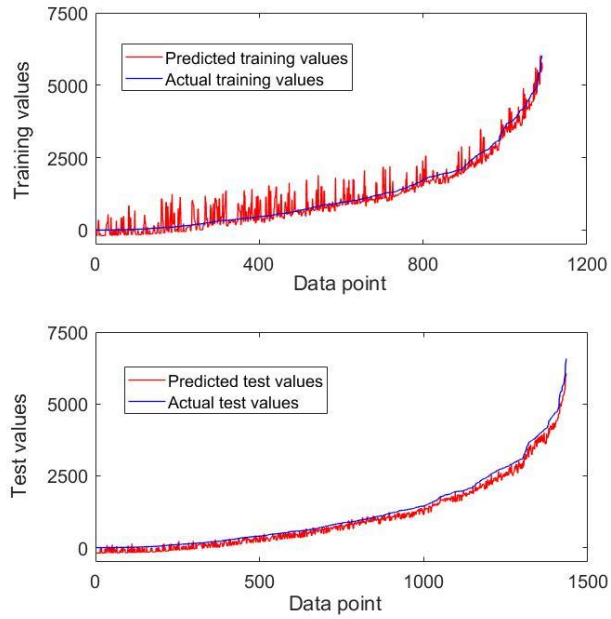

(b)

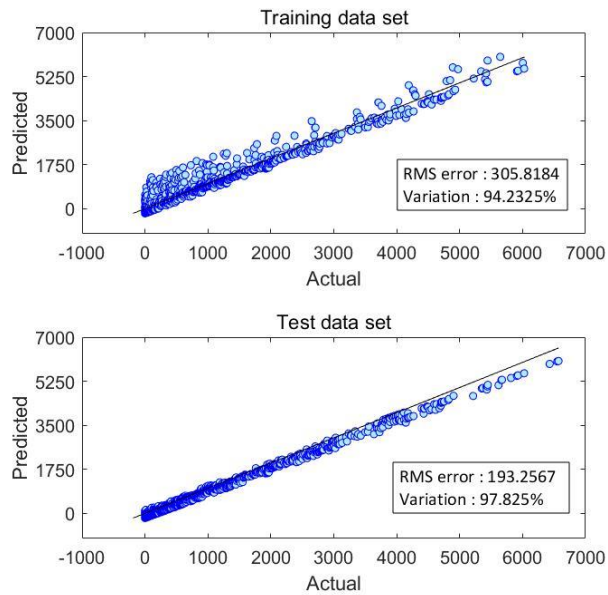

Figure 5.21 GP prediction performance of data-processed initial yield database based on reference simulations (training data for upper plot and test data for the bottom plots); (a) data-output plot, and (b) actual − predicted graph

Considering the results from Figure 5.20 and Figure 5.21, we confirmed that the GP is capable of generating a proper anisotropic yield criterion without any anisotropic parameters ($F, G, H,$ and N). The GP driven anisotropic yield surface shows reasonable results comparing with Hill's anisotropic yield criterion.

5.8. Self-Learning Data-Driven Anisotropic Yield Criterion from SELIFE Simulations

Next, based on the data-processed initial yield stress data from the self-learned stress-strain curves, other equation (28) can be obtained from the GP.

$$0.2922\sigma_{22}^2 + 0.2346\,\sigma_{11}^2 + 0.7345(\sigma_{11}\text{-}\sigma_{22})^2 + 3.1563\sigma_{12}^2 = \sigma_{yo}^2 \qquad \textbf{(28)}$$

Though the parameters characterizing anisotropic yield behavior are slightly different comparing with equation (27), equation (28) is able to produce reasonable elliptic shape. The other anisotropic yield surface from equation (28) is displayed in the stress space $\{\sigma_{11}, \sigma_{22}, \sigma_{12}\}$ and on the stress plane $\{\sigma_{11}, \sigma_{22}\}$ for the detail comparison with Hill's anisotropic yield surface in Figure 5.22 (a) and (b), respectively.

(a)

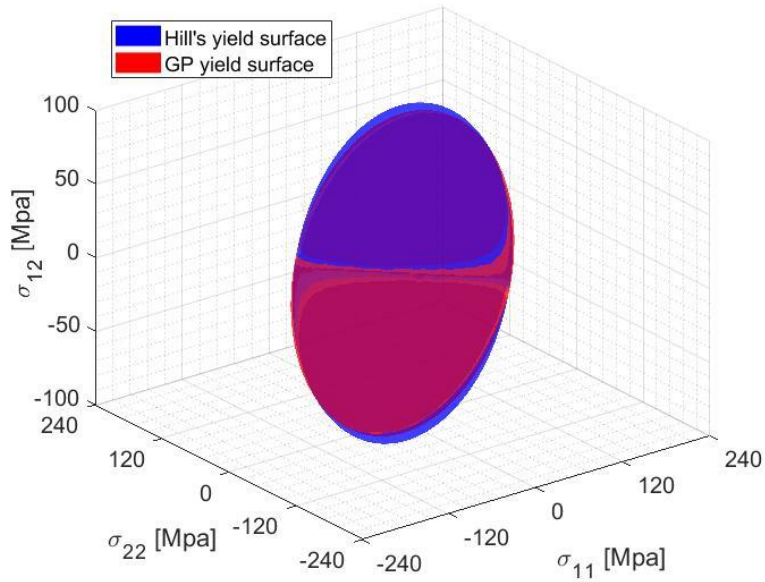

(b)

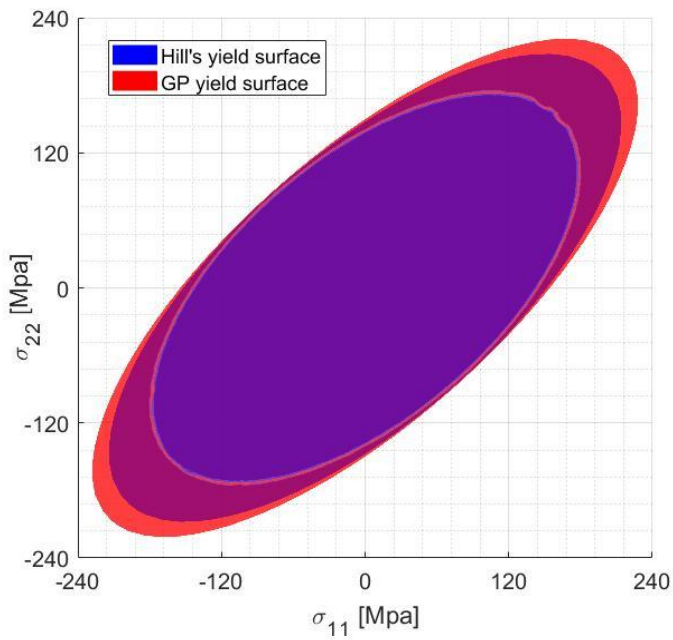

Figure 5.22 Comparison of anisotropic yield surfaces; (a) in the 3D stress space and (b) on the 2D stress plane

The prediction performance of the GP slightly decreased when the database were based on the SELIFE as shown in Figure 5.23. Using the SELIFE simulations, however, is meaningful since it can find stress and strain data from the unknown material with minimal mechanical properties. In this thesis, young's elastic modulus, poisson's ratio, and the initial yield stress of given material were only used in order to develop the GP-driven anisotropic yield criterion.

(a)

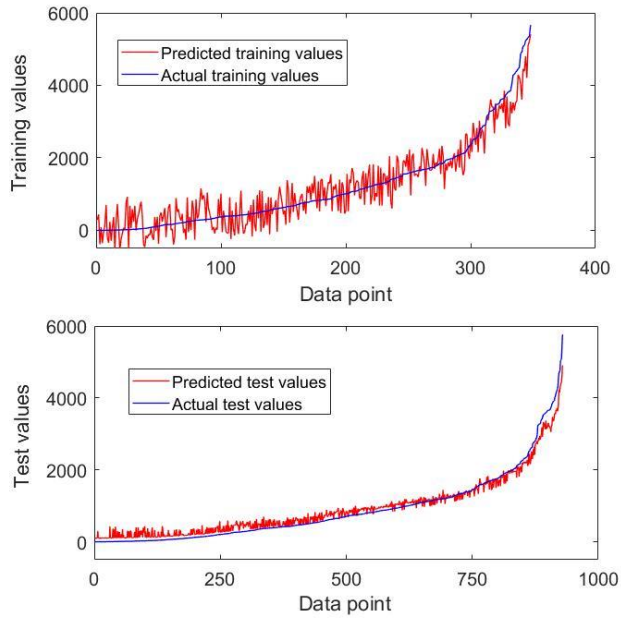

(b)

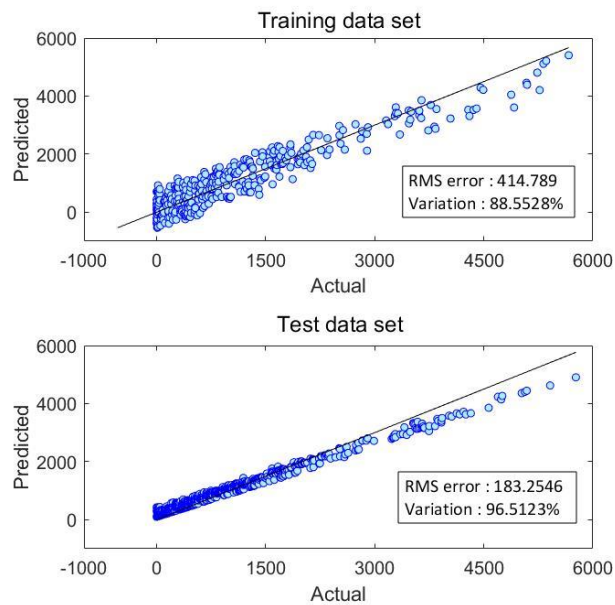

Figure 5.23 GP prediction performance of data-processed initial yield database based on SELIFE simulations (training data for upper plot and test data for the bottom plots); (a) data-output plot, and (b) actual − predicted graph

5.9. Verification of the GP Driven Yield Criterion

Based on the anisotropic parameters ($F, G, H,$ and N) of the GP driven equations i.e. equation (27), equation (28), measured yield stress can be obtained by equation (20), (21), and (24). Then, yield stress ratios (R_{11}, R_{22}, and R_{12}) were calculated following by equation (12) and are arranged in Table 5-9. Comparing with the original yield stress ratios, both groups of yield stress ratios were calculated similarly. Especially, the obtained yield stress ratios from the GP data driven equation Table 5-9 is close to the values of original yield stress ratios.

Table 5-9 Calculated yield stress ratios (R_{11}, R_{22}, and R_{12})

	R_{11}	R_{22}	R_{12}
Original material from Table 5-3 and (17)	1.0000	0.9715	1.0909
GP data driven equation (27)	0.9960	0.9671	1.0320
GP data driven equation (28)	1.0158	0.9869	0.9750

To verify the GP-driven yield equations, the other simulations were conducted with 22.5 degree of material orientation in ABAQUS. The calculated anisotropic yield stress ratios in Table 5-9 were used

for the verification simulations. Three lines are plotted together. All black solid lines are the results of the simulation with anisotropic yield criterion based on the original material given in Table 5-3. However, all blue lines are the results from the simulation based on the GP driven anisotropic yield equation (27) which is based on the initial yield stresses extracted from four reference simulations, and all red lines are the results from the simulation with the GP driven anisotropic yield criterion (28) which is stemmed from the initial yield stresses from four SELIFE.

The simulation with tension-tension displacement boundary condition was executed with 0.01[mm] displacement for the verification. Force-displacement data were extracted from the Region A and Region B and Figure 5.24 shows force-displacement comparison.

(a)

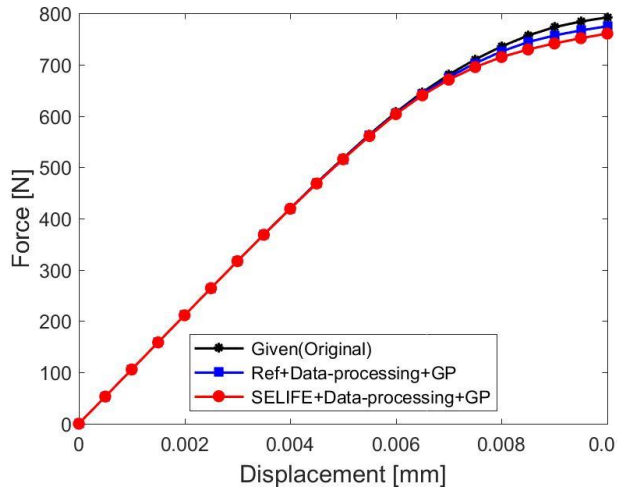

(b)

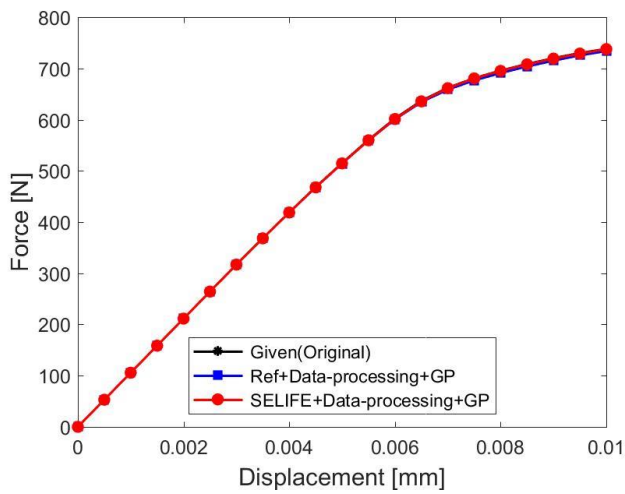

Figure 5.24 Force-displacement comparison from (a) the Region A and (b) the Region B

Moreover, stress-strain data were obtained from the specific elements and those are shown in Figure 5.25, Figure 5.26, and Figure 5.27. For elastic behavior case (Figure 5.25), there is no significant

difference among stress–strain curves. For plastic behavior case, however, slightly different plastic behavior appears in Figure 5.26 and Figure 5.27. It is based on the inherent error during the GP training as seen in Figure 5.23 (b) but stress history data had a similar material behavior comparing with the simulation with original anisotropic parameters.

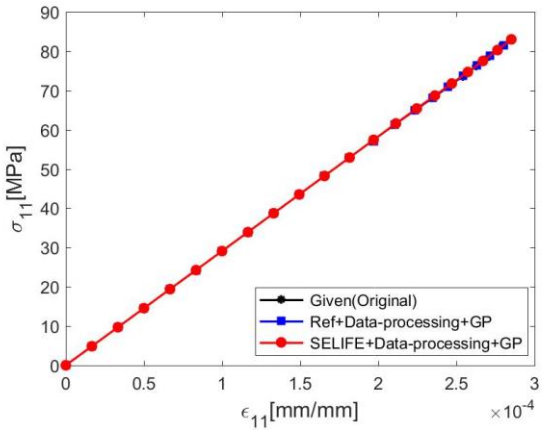

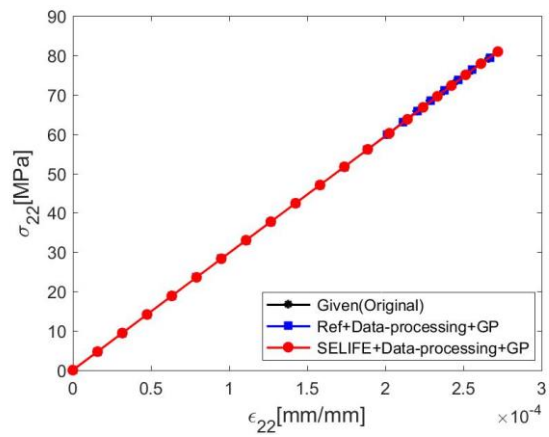

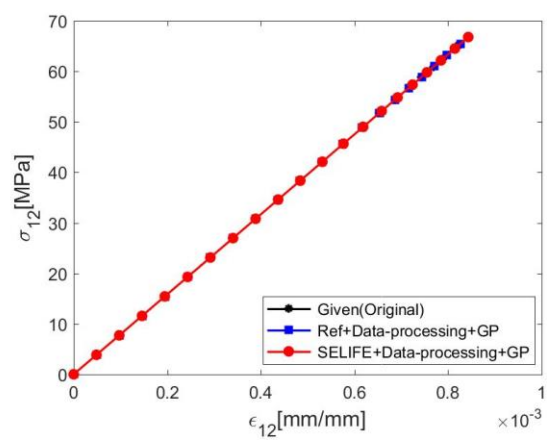

Figure 5.25 Comparison of stress-strain curves at the 2nd gauss point in the 51st element

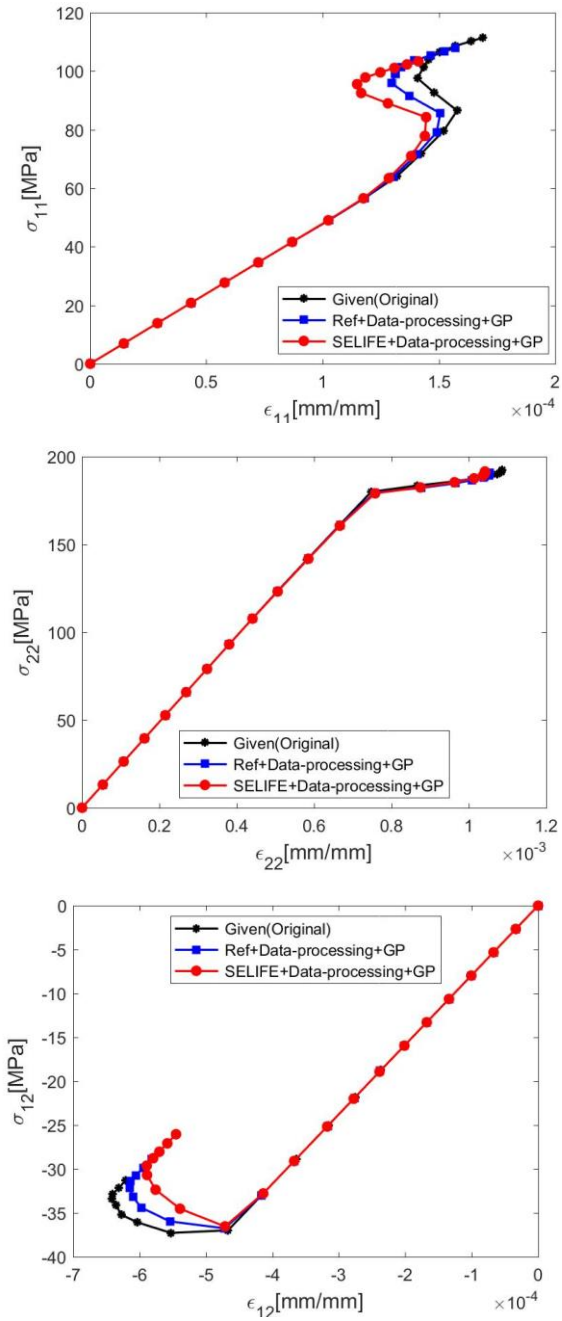

Figure 5.26 Comparison of stress-strain curves at the 4th gauss point in the 338th element

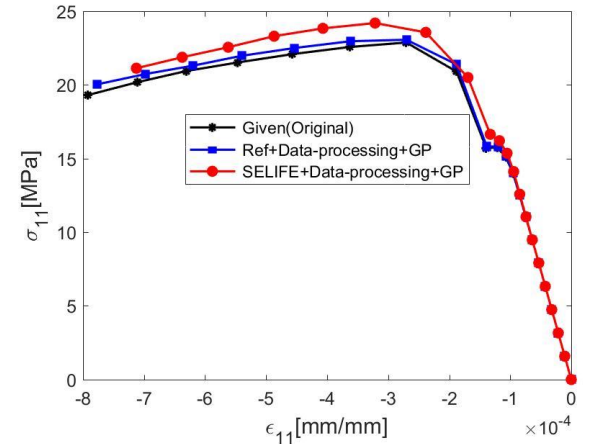

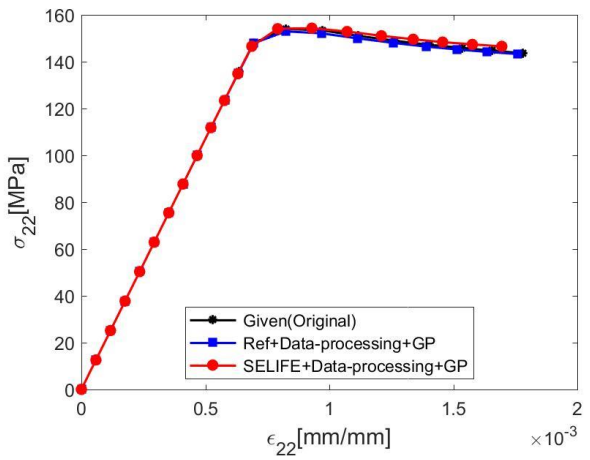

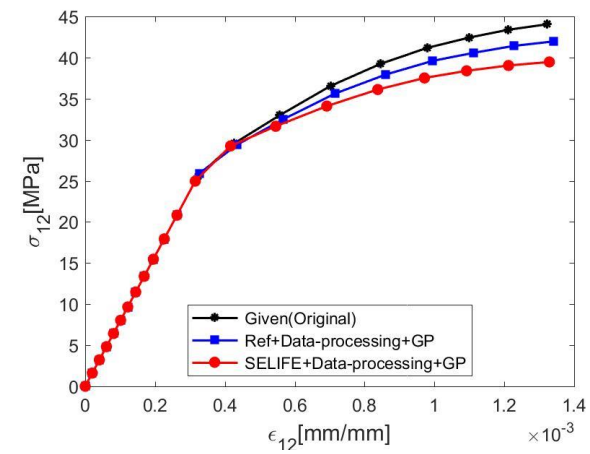

Figure 5.27 Comparison of stress-strain curves at the 3rd gauss point in the 186th element

6. Conclusion and Future Works

6.1. Conclusion

This thesis presented a novel methodology which is able to establish criteria from unknown material. The methodology mainly consist of data-driven approach i.e. self-learning inverse finite element (SELIFE) simulation, Data-processing, and genetic programming (GP). SEFIFE was able to gradually learn any material behavior based on the experimental measurements. Data-processing could find most of the initial yield stress points without any conventional yield criteria. Lastly, GP was capable of generating certain criteria in terms of the data-processed data.

In order to get sufficient initial yield stresses under various stress states, the biaxial specimen was modeled and simulated with four displacement boundary conditions: Tension-Tension, Compression-Compression, Compression-Tension, and Tension-Compression. Hill's 48 anisotropic yield criterion was assumed for the material behavior. Furthermore, experimental test data were substituted with the resultant force and displacement from the reference simulations which contain anisotropic yield behavior.

SELIFE simulations were carried out with the four displacement boundary conditions. The comparison of data curves illustrates that SELIFE is able to track the each of the corresponding target curves from repetitive stress-strain data learning. Effect of appending stress-strain data from FEM-A and FEM-B at the each of the loading steps allows artificial neural network to demonstrate more complex material behavior.

Initial yield stresses were generally captured by the Data-processing algorithm. Those initial yield data plotted on the Hill's yield surface. Most of the data appeared near to the Hill's yield surface. Genetic programming was capable of formulate anisotropic yield equation without any anisotropic parameters. Moreover, new anisotropic yield surface was plotted based on the driven equation. The new yield surface had similar elliptic shape comparing with the Hill's yields surface.

From unknown material, the proposed methodology could discover not only curves, that is, reaction force-displacement curve and stress-strain curve but also anisotropic yield criterion. Force-displacement curve and stress-strain curve were obtained during

the SELIFE based analysis. As NN pass increasing, trained ANN is getting to be helpful to execute nonlinear finite element analysis. Anisotropic yield criterion, however, were discovered from the symbolic regression by means of the GP.

6.2. Future Works

The GP results from the data based on the four reference simulations tended to be more accurate than those from the SELIFE. It means that more accurate stress-strain prediction of the SELIFE is required to achieve more precise anisotropic yield parameters and have more reasonable anisotropic yield surface. To overcome this limitation, more than one history will be included to improve the performance of stress prediction. Furthermore, state-of-the-art technique for Deep Learning will be accepted such as ADAM optimizer [39] and batch normalization [40]. Those technique is possible to enhance ANN accuracy with less computing time.

The proposed methodology will be extended to other anisotropic yield criteria researched by Hill [3-5], Bassani [6], and Budiansky [7]. Instead of using only a biaxial specimen, more complex stress behaviors can be considered by a triaxial experimental test [41].

Criteria can be developed with multiple stress components together from the test. Moreover, it will be applied to composite structures to establish failure criteria such as Tsai–Hill criterion or Tsai–Wu criterion [42].

7. Reference

[1] R. Von Mises, "Göttingen Nachrichten, Math," *Phys. Klasse,* vol. 582, 1913.

[2] W. Hosford, "A generalized isotropic yield criterion," *Journal of Applied Mechanics,* vol. 39, no. 2, pp. 607-609, 1972.

[3] R. Hill, "Theoretical plasticity of textured aggregates," in *Mathematical Proceedings of the Cambridge Philosophical Society*, 1979, vol. 85, no. 1: Cambridge University Press, pp. 179-191.

[4] R. Hill, *The mathematical theory of plasticity*. Oxford university press, 1998.

[5] R. Hill, "Constitutive modelling of orthotropic plasticity in sheet metals," *Journal of the Mechanics and Physics of Solids,* vol. 38, no. 3, pp. 405-417, 1990.

[6] J. Bassani, "Yield characterization of metals with transversely isotropic plastic properties," *International Journal of Mechanical Sciences,* vol. 19, no. 11, pp. 651-660, 1977.

[7] B. BUDIANSKY, "Anisotropic plasticity of plane-isotropic sheets," in *Studies in Applied Mechanics*, vol. 6: Elsevier, 1984, pp. 15-29.

[8] T. Kirchdoerfer and M. Ortiz, "Data-driven computational mechanics," *Computer Methods in Applied Mechanics and Engineering,* vol. 304, pp. 81-101, 2016.

[9] F. Abbassi, T. Belhadj, S. Mistou, and A. Zghal, "Parameter identification of a mechanical ductile damage using Artificial Neural Networks in sheet metal forming," *Materials & Design,* vol. 45, pp. 605-615, 2013.

[10] K. Rajan, "Materials informatics: The materials "gene" and big data," *Annual Review of Materials Research,* vol. 45, pp. 153-169, 2015.

[11] H. Ohno, "Uniforming the dimensionality of data with neural networks

for materials informatics," *Applied Soft Computing,* vol. 46, pp. 17-25, 2016.
[12] R. Ramprasad, R. Batra, G. Pilania, A. Mannodi-Kanakkithodi, and C. Kim, "Machine learning in materials informatics: recent applications and prospects," *npj Computational Materials,* vol. 3, no. 1, p. 54, 2017.
[13] L. Wang, *Support vector machines: theory and applications*. Springer Science & Business Media, 2005.
[14] C. M. Breneman *et al.*, "Stalking the Materials Genome: A Data-Driven Approach to the Virtual Design of Nanostructured Polymers," *Advanced functional materials,* vol. 23, no. 46, pp. 5746-5752, 2013.
[15] H. DV, S. Itoh, T. Sakai, S. Kamado, and Y. J. M. t. Kojima, "Experimentally and numerical study on deep drawing process for magnesium alloy sheet at elevated temperatures," vol. 49, no. 5, pp. 1101-1106, 2008.
[16] S. R. Kalidindi, S. R. Niezgoda, and A. A. Salem, "Microstructure informatics using higher-order statistics and efficient data-mining protocols," *Jom,* vol. 63, no. 4, pp. 34-41, 2011.
[17] T. Furukawa and M. Hoffman, "Accurate cyclic plastic analysis using a neural network material model," *Engineering Analysis with Boundary Elements,* vol. 28, no. 3, pp. 195-204, 2004.
[18] R. Haj-Ali and H.-K. Kim, "Nonlinear constitutive models for FRP composites using artificial neural networks," *Mechanics of Materials,* vol. 39, no. 12, pp. 1035-1042, 2007.
[19] Y. Shen, K. Chandrashekhara, W. Breig, and L. Oliver, "Neural network based constitutive model for rubber material," *Rubber chemistry and technology,* vol. 77, no. 2, pp. 257-277, 2004.
[20] S. Jung and J. Ghaboussi, "Characterizing rate-dependent material behaviors in self-learning simulation," *Computer methods in applied mechanics and engineering,* vol. 196, no. 1-3, pp. 608-619, 2006.
[21] J. Ghaboussi, J. Garrett Jr, and X. Wu, "Knowledge-based modeling of material behavior with neural networks," *Journal of engineering mechanics,* vol. 117, no. 1, pp. 132-153, 1991.
[22] T. Furukawa and G. Yagawa, "Implicit constitutive modelling for viscoplasticity using neural networks," *International Journal for Numerical Methods in Engineering,* vol. 43, no. 2, pp. 195-219, 1998.
[23] J. Ghaboussi and D. Sidarta, "A new nested adaptive neural network for modeling of constitutive behavior of materials," *International Journal of Computer and Geotechnics,* vol. 22, no. 1, pp. 29-51, 1998.
[24] J. Ghaboussi and D. Sidarta, "New nested adaptive neural networks (NANN) for constitutive modeling," *Computers and Geotechnics,* vol. 22, no. 1, pp. 29-52, 1998.
[25] G. Liang and K. Chandrashekhara, "Neural network based constitutive

model for elastomeric foams," *Engineering Structures,* vol. 30, no. 7, pp. 2002-2011, 2008.

[26] G. Yun, J. Ghaboussi, and A. Elnashai, "Neural network-based constitutive model for cyclic behavior of materials," in *The First European Conference on Earthquake Engineering and Seismology*, 2006.

[27] Y. Hashash, S. Jung, and J. Ghaboussi, "Numerical implementation of a neural network based material model in finite element analysis," *International Journal for numerical methods in engineering,* vol. 59, no. 7, pp. 989-1005, 2004.

[28] J. Ghaboussi, D. A. Pecknold, M. Zhang, and R. M. Haj-Ali, "Autoprogressive training of neural network constitutive models," *International Journal for Numerical Methods in Engineering,* vol. 42, no. 1, pp. 105-126, 1998.

[29] A. H. Gandomi and G. J. Yun, "Coupled SelfSim and genetic programming for non-linear material constitutive modelling," *Inverse Problems in Science and Engineering,* vol. 23, no. 7, pp. 1101-1119, 2015.

[30] G. J. Yun, J. Ghaboussi, and A. S. J. I. J. f. N. M. i. E. Elnashai, "A new neural network-based model for hysteretic behavior of materials," vol. 73, no. 4, pp. 447-469, 2008.

[31] M. Riedmiller and H. Braun, "A direct adaptive method for faster backpropagation learning: The RPROP algorithm," in *Proceedings of the IEEE international conference on neural networks*, 1993, vol. 1993: San Francisco, pp. 586-591.

[32] G. J. Yun, A. Saleeb, S. Shang, W. Binienda, and C. J. J. o. A. E. Menzemer, "Improved selfsim for inverse extraction of nonuniform, nonlinear, and inelastic material behavior under cyclic loadings," vol. 25, no. 2, pp. 256-272, 2011.

[33] G. J. Yun, J. Ghaboussi, and A. S. Elnashai, "Self-learning simulation method for inverse nonlinear modeling of cyclic behavior of connections," *Computer methods in applied mechanics and engineering,* vol. 197, no. 33-40, pp. 2836-2857, 2008.

[34] D. P. Searson, D. E. Leahy, and M. J. Willis, "GPTIPS: an open source genetic programming toolbox for multigene symbolic regression," in *Proceedings of the International multiconference of engineers and computer scientists*, 2010, vol. 1: Citeseer, pp. 77-80.

[35] Y. Bao, "Dependence of ductile crack formation in tensile tests on stress triaxiality, stress and strain ratios," *Engineering fracture mechanics,* vol. 72, no. 4, pp. 505-522, 2005.

[36] Y. Choi, C.-S. Han, J. K. Lee, and R. H. Wagoner, "Modeling multi-axial deformation of planar anisotropic elasto-plastic materials, part

I: Theory," *International Journal of Plasticity,* vol. 22, no. 9, pp. 1745-1764, 2006/09/01/ 2006.

[37] R. J. P. o. t. R. S. o. L. S. A. M. Hill and P. Sciences, "A theory of the yielding and plastic flow of anisotropic metals," vol. 193, no. 1033, pp. 281-297, 1948.

[38] S. Bagherzadeh, M. Mirnia, and B. M. Dariani, "Numerical and experimental investigations of hydro-mechanical deep drawing process of laminated aluminum/steel sheets," *Journal of Manufacturing Processes,* vol. 18, pp. 131-140, 2015.

[39] D. P. Kingma and J. Ba, "Adam: A method for stochastic optimization," *arXiv preprint arXiv:1412.6980,* 2014.

[40] S. Ioffe and C. Szegedy, "Batch normalization: Accelerating deep network training by reducing internal covariate shift," *arXiv preprint arXiv:1502.03167,* 2015.

[41] S. Calloch and D. Marquis, "Triaxial tension-compression tests for multiaxial cyclic plasticity," *International Journal of Plasticity,* vol. 15, no. 5, pp. 521-549, 1999.

[42] S. W. Tsai and E. M. Wu, "A general theory of strength for anisotropic materials," *Journal of composite materials,* vol. 5, no. 1, pp. 58-80, 1971.

국문초록

비등방성 재료에 대한 자가 학습 데이터 기반의 항복 조건

장 경 석
기계항공공학부
서울대학교 대학원

항복 기준은 원하지 않은 물질적 거동을 막기 위한 구조 분석에 필수적인 이론 중 하나이다. 비록 이 이론들이 높은 정확도로 개발되었지만, 비등방성 항복 기준식을 완성하기 위해서는 많은 비등방성 변수가 필요하다. 그리고 비등방성 물질의 불확실성으로 인해 많은 실험 테스트가 필요하다. 본 논문의 주요 목적은 특징 없는 새로운 물성의 비등방성 항복 기준을 식별할 수 있는 새로운 방법론을 제안하는 것이다. 새로운 방법론은 1) 최소한의 실험 측정을 통한 자기 학습 유한 요소 SELIFE 시뮬레이션과 2) 데이터 기반 역학 접근의 두 가지 단계를 통해 새로운 항복 기준을 생성한다. SELIFE는 경계 힘 조건, 경계 변위 조건 및/또는 실험으로부터 내부 변위에 기초한 모든 물질 거동의 응력-변형 시간 이력을 스스로 학습할 수 있다. SELIFE 분석에서 물질 거동의 자기 학습 능력은 인공신경망 기반 물질 구성

모델의 적응적 진행적 훈련을 통해 활성화된다. 자체 학습된 응력-변형률 데이터로부터, 충분한 초기 항복 응력을 포괄적인 응력 증가 방향으로 추출했다. 이것을 데이터 처리 단계라고 한다. 데이터 처리 이후에는 새로운 데이터 기반 비등방성 항복 기준을 도출하기 위해 유전자 프로그래밍을 통한 심볼릭 회귀 분석을 수행한다. 예를 들어, Hill의 비등방성 항복 기준식이 사용되는데, 이 기준식은 알려지지 않은 것으로 가정한다. 충분하고 다양한 초기 항복 응력 데이터를 얻기 위해 이축 시편에 4개의 변위 경계 조건을 적용하여 시뮬레이션 하였다. 마지막으로, ABAQUS에 데이터 기반 항복 기준식을 사용하여 이축 시뮬레이션이 실행되었다. SELIFE 시뮬레이션과 데이터 기반 역학 접근법을 통해 새로운 비등방성 항복 기준식을 얻어 기준 항복 기준식과 비교했다.

Keywords : 데이터 기반 , 인공신경망, 유전자 프로그램, 비등방성 항복 기준, 초기 항복 응력, 이축 시편

Student Number : 2017-27307